Editors' Suggestion

Exactly solvable flat-foldable quadrilateral origami tilings

Michael Assis
School of Mathematics and Statistics, University of Melbourne, Parkville, Victoria 3010, Australia

(Received 24 May 2017; revised manuscript received 8 August 2018; published 7 September 2018)

We consider several quadrilateral origami tilings, including the Miura-ori crease pattern, allowing for crease-reversal defects above the ground state which maintain local flat foldability. Using exactly solvable models, we show that these origami tilings can have phase transitions as a function of crease state variables, as a function of the arrangement of creases around vertices, and as a function of local layer orderings of neighboring faces. We use the exactly solved cases of the staggered odd eight-vertex model as well as Baxter's exactly solved three-coloring problem on the square lattice to study these origami tilings. By treating the crease-reversal defects as a lattice gas, we find exact analytic expressions for their density, which is directly related to the origami material's elastic modulus. The density and phase transition analysis has implications for the use of these origami tilings as tunable metamaterials; our analysis shows that Miura-ori's density is more tunable than Barreto's Mars density, for example. We also find that there is a broader range of tunability as a function of the density of layering defects compared to as a function of the density of crease order defects before the phase transition point is reached; material and mechanical properties that depend on local layer ordering properties will have a greater amount of tunability. The defect density of Barreto's Mars, on the other hand, can be increased until saturation without passing through a phase transition point. We further consider relaxing the requirement of local flat foldability by mapping to a solvable case of the 16-vertex model, demonstrating a different phase transition point for this case.

DOI: 10.1103/PhysRevE.98.032112

I. INTRODUCTION

Recently, foldable origami crease patterns (CPs) have seen much use as programmable matter [1,2], tunable metamaterials [3,4], self-deployable systems [5,6], architecture [7], and medical devices [8–11]. In many of these explorations, the origami CP hinges are self-folding after application of heat [12,13], electric current [1,2,5], lasers [14], and various liquids [15], to name some examples. See [16] for a recent review.

In [3] the authors show experimentally how the elastic modulus of a Miura-ori origami CP depends on the density of defects present, that is, the number of creases with opposite orientations than the original CP. Defects can also arise in the production of reversible self-folding origami based on hydrogel bilayers [17], and in [5] the authors report that initially some creases started self-folding in the opposite orientation before correcting themselves. Presumably, defects naturally arise after several cycles of reversible self-folding and unfolding and they certainly arise through environmental factors. Along these lines, there has been recent interest in finding the minimum number of crease orientations necessary to force the orientations of the remaining creases in the lattice as the origami CP is being activated, the so-called forcing sets [18,19]; due to multistability, however, defects can easily arise from forcing sets [20,21].

We are interested in characterizing flat-foldable defects which can arise in origami CPs, and so we here study origami CPs from the perspective of exactly solvable equilibrium statistical mechanics. Our statistical ensembles are presumed to be either a large collection of manufactured origami CPs, self-folding once to their final shape or else a single origami undergoing many cycles of reversible self-folding and unfolding, in which case it would approach equilibrium after a number of such cycles. We do not consider localized tuning of creases on the lattice, such as forcing sets, but rather use homogeneous variables throughout the lattice and assume that all creases must be folded. Our exact solutions allow us to derive not only exact phase transition point locations, but also free-energy expressions which allow the derivation of its thermodynamical properties.

The nature of this work bridges the theoretical models of exactly solvable lattice statistical mechanics with the more experimental work on origami engineering, condensed matter physics, and materials science. We do not assume a familiarity with all of these areas and attempt to explain a sufficient amount of origami results and theory in order to both allow the statistical mechanics theorists to understand the applications of the models to origami and explain sufficiently the methods and models of statistical mechanics to those not familiar with the exactly solved models. Those more familiar with origami and more interested in the applications of the theory may wish to skip some details of the models and focus on Secs. VI and VIII, while those not familiar with origami and its applications may wish to spend more time studying the Introduction and Secs. II and III.

In our models, the ground state represents a known origami CP crease configuration and excitations above the ground state represent defects in the foldable lattice due to reversal of the states of the creases, from mountain to valley or vice versa. The phase transitions of our models represent points at which the long-range order in the lattice disappears, either with respect to crease states in the lattice or else with respect

FIG. 1. Mapping of mountain folds to solid lines (left) and valley folds to dashed lines (right).

to relative face layer orderings, which is the ordering of the stacking of faces locally after folding, so that correlations of either of these variables decay exponentially above the phase transition point. As a consequence of our analysis, we are able to characterize CPs which are more stable against defects than others and, conversely, which are more tunable as a metamaterial. Some CPs do not feature a phase transition point and so defects can be added to the lattice until saturation without changing its long-range-order properties. Our models enable us to predict the defect density as a function of the preference of creases for the reversed state. To the extent that mechanical properties of the origami CP depend on the defect density, knowledge of how much to bias the creases in the lattice allows for a tuning of the defect density and hence of the mechanical properties.

Origami CPs readily lend themselves to vertex model interpretations in statistical mechanics. If we represent mountain creases by solid lines and valley creases by dashed lines as in Fig. 1, then we have a direct correspondence with vertex models with two-state edges, having Boltzmann weights $v_i = \exp(-\beta\varepsilon_i)$ defined in terms of the configuration of mountain and valley creases around a vertex in the lattice, where ε_i represents an interaction energy or chemical potential and $\beta = (k_B T)^{-1}$, where k_B is Boltzmann's constant and T is the temperature. With these definitions, we sum over all of the possible valid vertex configurations in the lattice to arrive at the partition function Z,

$$Z = \sum_{\text{configs}} \prod_i v_i^{m_i}, \tag{1}$$

where m_j are the number of vertex weights v_i in the lattice. In the thermodynamic limit where the number of lattice sites $\mathcal{N} \to \infty$, the free energy f is defined by

$$-\beta f = \lim_{\mathcal{N}\to\infty} \ln(Z^{1/\mathcal{N}}). \tag{2}$$

From the free energy, all thermodynamic quantities and critical phenomena can be derived.

Vertex models in statistical mechanics are often defined on a regular lattice. The lattice edge lengths and angles are typically disregarded; only the graph connectivity of vertices is usually of interest. For origami CPs, on the other hand, not only the graph but the angles and edge lengths are important for its foldability properties. In particular, necessary flat-foldability conditions require that the alternating sum of angles around a vertex add to π (Kawasaki's theorem), that each vertex be of even degree, and that the difference in the number of mountain and valley creases around each vertex equal two (Maekawa's theorem) [22]. Also, changing the angles of creases around a vertex can change the number of valid mountain-valley crease assignments which are flat-foldable around that vertex, even while still satisfying Kawaski's theorem at that vertex. Therefore, since we are interested in changing crease assignments to allow for defects, we must also incorporate the effect of the CP angles on the number of allowed crease assignments around a vertex into our models. Furthermore, aside from the importance of angles in flat foldability and determining the number of valid crease assignments, flat-foldable CPs with the same connectivity and the same crease assignments but different angles can have very different folding properties, as seen in [23], where the Miura-ori, Barreto's Mars, the quadrilateral mesh, and the dual square twist CPs only differ in their angles, even though their resulting global foldings are quite different. We will not directly consider the resulting folding of the CP.

Sufficient conditions for the global flat foldability of an origami CP is an NP-hard problem [24], depending on the global layer ordering of the facets. This layer ordering condition can in principle be translated into a statistical mechanics model, by mapping to a solid on solid (SOS) model with a partial height ordering around each vertex and summing over those configurations which admit a global height ordering. As far as we are aware, this kind of model cannot be reduced to only nearest-neighbor interactions. We therefore do not consider global flat foldability. Because of the inherent difficulty of dealing with global flat-foldability conditions, we will only consider local flat-foldability requirements. Furthermore, we do not assume rigid flat faces during folding but assume that during folding the faces can bend before settling down to a final (locally at least) flat-foldable state; we discuss rigid foldability in Sec. VIII.

Ours is not the first attempt to relate origami crease patterns to statistical mechanics. Most other work has been done considering foldings of polymerized membranes or tethered membranes on a lattice, that is, random crumplings of the lattice where not all bonds need to be folded. See [25] for such a study on the square lattice, [26–37] for studies on the triangular lattice, and [38–40] for studies on the union-jack lattice. Also, one-dimensional folding as a meander problem was considered in [41,42]. In [43,44] foldings of all edges of triangulations by regular triangles of arbitrary genus surfaces were considered, but since their only restrictions were even degree vertices which were three-colorable, in order to allow the mapping of all triangular faces onto each other, they disregarded Kawasaki and Maekawa's theorems. See [45–47] for reviews on these topics just mentioned. We also note [48], where a mapping was given from the kagome lattice Heisenberg antiferromagnet to a folded triangular sheet. Except for the exact calculation of the folding entropies of random crumpling on a triangular lattice [49] and of flat-foldable Miura-ori states [50], we are unaware of other exact results. Our work here uses exactly solvable models to study origami CPs in general.

As a means of studying origami CPs using the methods of solvable equilibrium statistical mechanics, we will confine ourselves in this paper to origami CPs whose graph connectivities are of the form of a square lattice, that is, regular degree four lattices. We consider staggering units of up to four vertices in our models of isohedral quadrilateral tilings of the plane which are flat foldable. These flat-foldable tilings are the simple square tiling, the parallelogram or rhombus (pmg) tiling commonly known as Miura-ori, the trapezoid tiling, called chicken wire in [23], and the kite tiling, called Huffman in [23], where we use the International Union of Crystallography

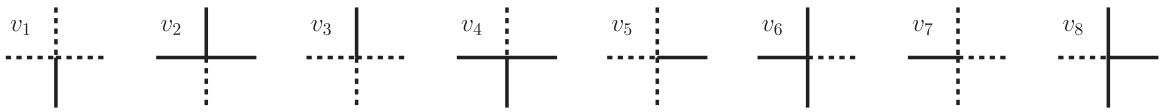

FIG. 2. Odd eight-vertex model weights, with bond states shown in terms of line type, dashed or solid, representing valley or mountain creases, respectively.

short crystallographic notation for the wallpaper groups to distinguish Miura-ori from the parallelogram p2 and rhombus cmm tilings. We will use the standard naming conventions of the trapezoid and kite tiling but use the Miura-ori name, which is well known in the origami literature, rather than the parallelogram or rhombus pmg tiling naming convention; we will also refer to the square tiling as the simple square CP.

In our translation of the CPs to our square lattice models we impose the flat-foldability restrictions inherent in the origami CP due to the values of its angles. We will generally only consider locally flat-foldable origami CPs, except when looking at CPs which break Maekawa's theorem at vertices. Since we are not considering global flat foldability, it is possible that some of the configurations of crease assignments which are included in the partition function summation are not globally flat foldable. We also do not consider rigid foldability but assume that faces can bend. Indeed, the ground-state crease assignment of the trapezoid CP can self-intersect globally if only rigid foldability is being considered [51]; the ground state is globally flat foldable however.

Maekawa's theorem applied to degree 4 vertices demands an odd number of mountain and valley creases. Thus there are eight valid locally flat-foldable vertex configurations at each square lattice vertex, shown in Fig. 2, which immediately recalls the odd eight-vertex model [52,53].

In the CPs we consider there is one continuous degree of freedom in their definitions, given in terms of an angle θ in the staggering quadrilateral unit, as shown in Fig. 3. For any angle $\theta < 90^\circ$, geometrical folding constraints force two or four vertex weights to be disallowed, that is, $v_i = 0$, in these CPs, as shown in Fig. 4. When the angle $\theta = 90^\circ$, all four CPs become degenerate with the homogeneous square lattice CP where all eight vertex weights v_i can be nonzero.

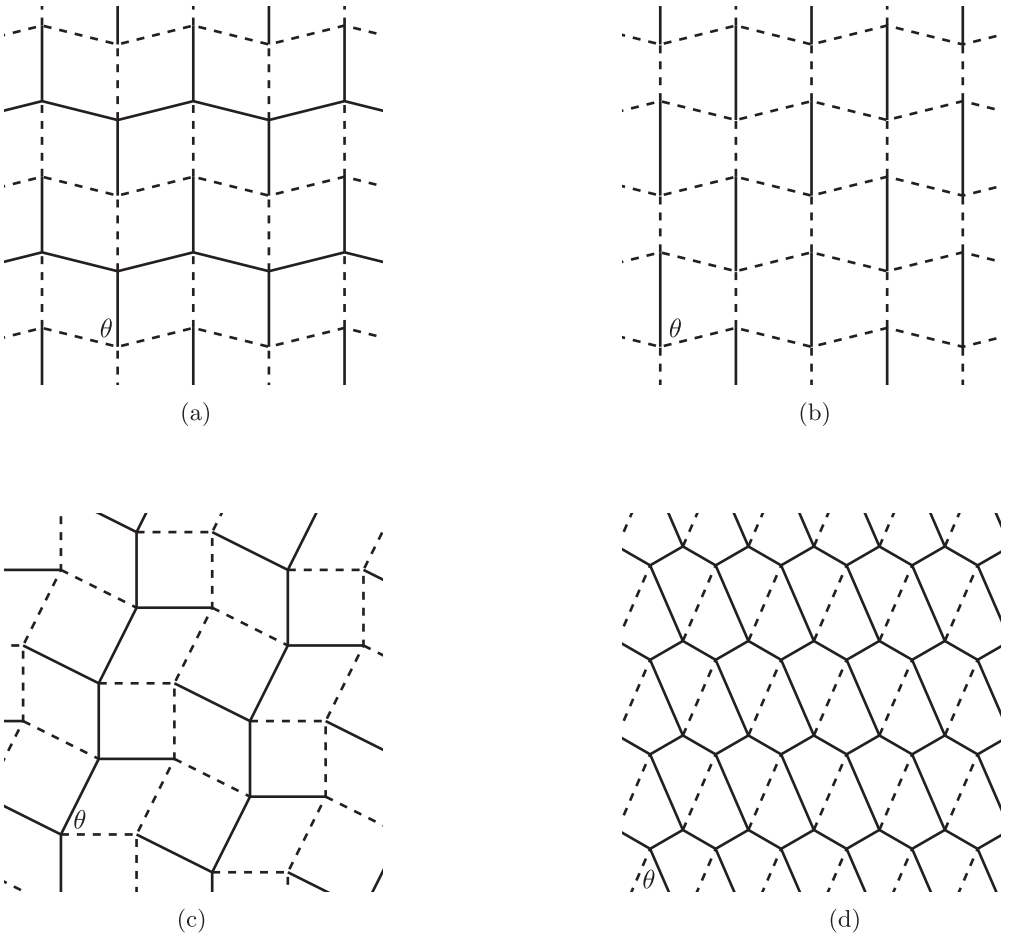

FIG. 3. Four of the five origami CPs we consider: (a) the Miura-ori CP, (b) the trapezoid CP, (c) Barreto's Mars CP, and (d) the kite CP; the simple square tiling is not shown.

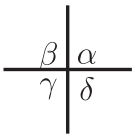

(a)

Angle pattern example	Disallowed weights	Representative CP
$\alpha = \beta < 90^\circ,\ \gamma = \delta = \alpha + 90^\circ$	$v_1 = v_2 = 0$	Miura-ori, trapezoid
$\alpha < 90^\circ,\ \gamma = \alpha + 90^\circ,\ \beta = \delta = 90^\circ$	$v_1 = v_2 = v_7 = v_8 = 0$	Barreto's Mars, kite
$\alpha = \beta = \gamma = \delta = 90^\circ$		Square

(b)

FIG. 4. (a) Single vertex with angles labeled and (b) dependence of the allowed flat-foldable vertex weights on the angle pattern examples.

Therefore, we will assume in talking about these CPs that $\theta \neq 90^\circ$.

From the perspective of allowed vertex weights at each vertex of the CP according to the table in Fig. 4, the Miura-ori CP is column staggered with units of two vertices, trapezoid and kite CPs are bipartite staggered with units of two vertices, and Barreto's Mars CP is column staggered with units of four vertices. However, as we will see below, it is more useful, in order to set the correct ground state, to consider the Miura-ori CP as a column staggered lattice with units of four vertices. Very few exact results are known for staggered vertex models, the majority being free-fermion eight-vertex models; the only solved staggered vertex models which are not free-fermion models have extra interactions which do not have a natural origami interpretation [53]. Therefore, we will focus on free-fermion models, which have simple solution constructions in terms of Pfaffian or dimer methods. Bipartite staggered even eight-vertex models with units of two vertices were studied in [54], column staggered even and odd eight-vertex models with units of two vertices were studied in [53], and column staggered even eight-vertex models with units of four vertices were considered in [55]. Because staggered even eight-vertex models can always be mapped to staggered odd eight-vertex models by reinterpreting bond occupation variables [52,53], we can make use of the results in these papers for our purposes. For reference, in Appendix A we give the dimer method of solution for the column staggered odd eight-vertex model with units of four vertices, from which all of the remaining vertex model results can be specialized. The free energies are given in Appendix B.

We find that the Miura-ori and trapezoid CPs have phase transition points as a function of the vertex weights, points beyond which the long-range order of the ground state disappears. We also find that Barreto's Mars CP has purely noninteracting defects and that the kite CP can be treated as an effective one-dimensional model. Therefore, neither Barreto's Mars nor kite CPs have a phase transition point. For the simple square CP, the equivalent homogeneous odd eight-vertex free-fermion model does not have a phase transition unless at least two of the vertex weights are disallowed at each vertex [52], but if we consider a staggering of two or four units, then there exist phase transitions for all positive weights, which we give in Sec. IV E.

The Miura-ori and trapezoid CPs can also be mapped to the exactly solved three-coloring problem on the square lattice [50,56–58], where colors represent relative layering orders of neighboring faces. The model does not allow two neighboring faces to have the same color, and the ground state is chosen to only have two colors in a checkerboard fashion. The introduction of the third color maps to the appearance of defects on the lattice. The three-coloring problem has a known phase transition which these two CPs also exhibit as a function of these face layer defects. Because the three-coloring problem does not satisfy the free-fermion condition, this is a phase transition point outside of those seen in the mapping to the staggered free-fermion odd eight-vertex model solutions, and it also happens for a different order parameter in the problem, namely, the relative local face layer orderings.

In Sec. VI we treat the models as a lattice gas of defects, and using the free-energy results, reinterpreted as pressure, we find exact analytic expressions for the density of defects in these models. We consider crease-reversal defects as "particles" as well as layer ordering defects. Our analysis of the densities allow us to conclude that Miura-ori and trapezoid densities are less stable against defects, and hence more tunable, than Barreto's Mars density. We also give analytic expressions for the isothermal compressibility and compute the equations of state of these lattice gas models.

Finally, we also consider relaxing the local flat-foldability requirement by breaking Maekawa's theorem on the simple square CP in Sec. VII. There are then a total of 16 valid vertex weights at each vertex and by imposing a crease reversal symmetry to the vertex weights, we make use of a weak-graph transformation to map this model to an even eight-vertex model with the known solvable subcase of the free-fermion model [53,59]. We find for this model another phase transition point. We discuss in Sec. VIII rigid foldability, finite lattice results, higher degree CPs, free-fermion models, and lattice versions of random crumpling. We finish the paper in Sec. IX with some conclusions.

II. FLAT-FOLDABLE CREASE-REVERSAL DEFECTS

The flat-foldability requirement about each vertex means that crease assignment defects cannot occur in isolation. In order to satisfy Maekawa's theorem, an even number of crease reversals from the ground state must occur at each vertex, either two or four, and since a crease joins two vertices, neighboring vertices are affected. The arrangement of angles in the CP further limits the number of possible crease reversals around a vertex. We show the valid types of crease reversals around vertices in Fig. 5, where we also indicate which types are valid for each CP.

From the valid crease reversals around each vertex, we can see that the kite's crease defects form lines which traverse the entire lattice and Barreto's Mars forms only small crease defect loops around the diamond faces of the CP which are independent of each other. The types of crease defects which occur in Miura-ori, trapezoid, and simple square CPs are more interesting and can interact with each other. For these three CPs, all finite terminating crease defects form loops enclosing polygonal areas which can be viewed as being composed of

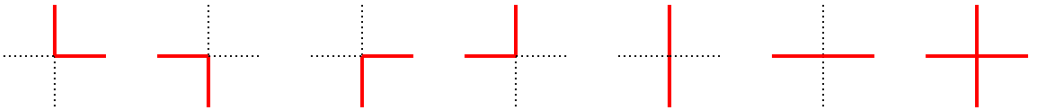

FIG. 5. Schematic representation of the valid crease reversals around vertices, with crease reversals indicated by solid red lines. All CPs admit the seventh type. In addition, the kite CP admits the first two types; Miura-ori, trapezoid, and Barreto's Mars CPs admit the first four types; and Barreto's Mars CP admits the first two only on one sublattice and the next two on the other sublattice only. The simple square CP admits all seven types.

a number of individual face defects that have been joined together. For these three CPs then, the finite-size defects have as their basic units what we call face flips, where all four creases around a face are reversed. All of the defects in Barreto's Mars have face flips as their building blocks, but the other CPs can also have isolated lines of defects which traverse the entire lattice which cannot be built up using only face-flip defects. In Fig. 6 we show a sample of possible face-flip defects for these models at low and high densities of crease reversals.

Though face flips are useful for understanding defects, except for Barreto's Mars it is important that the crease-reversal models use crease reversals as a defect variable and not face flips. At low density, the two cases will agree, but at high face-flip density the lattice will be covered by face flips, which is equivalent to the ground state and not the fully crease-reversed lattice. Since we are interested in characterizing the effect of defects in the lattice and want the high density to correspond to the lattice being fully crease reversed, we see that we cannot use face flips as a useful Boltzmann weight in these models. For Barreto's Mars, since the only allowed defects occur on the diamond faces and the defects are noninteracting, face flips are an equally valid Boltzmann weight and the model can be viewed as a noninteracting lattice gas of diamonds.

III. ORIGAMI BOLTZMANN WEIGHTS

Origami CPs fold in a manner which depends on the crease assignments, the arrangement of those creases around individual vertices, and the ordering of the layers of faces. We consider Boltzmann weights for each of these three cases, weights that depend on the arrangement of crease assignments around a vertex using the standard odd eight-vertex model weights shown in Fig. 2, individual crease Boltzmann weights for mountain and valley crease assignments separately, and relative layer ordering weights for faces with respect to their neighboring faces. We consider each type of weight in turn below.

A. Vertex Boltzmann weights and free-fermion models

If treated purely as a vertex model, the origami models then have Boltzmann weights which depend only on the pattern

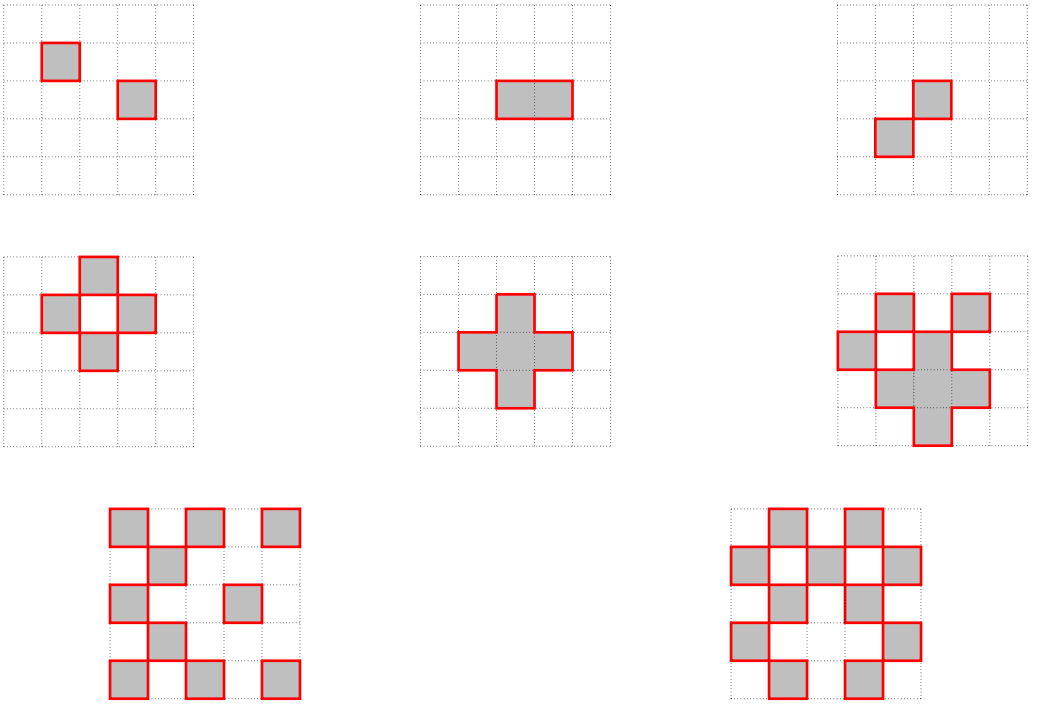

FIG. 6. Schematic representation of face-flip defect configurations, where solid red lines represent crease reversals for Miura-ori, trapezoid, Barreto's Mars, and the simple square CPs. The first two rows are at low density and the bottom row is at high density. The top middle configuration cannot occur except for the simple square CP, and Barreto's Mars face-flip defects only occur for its diamond faces.

of mountain and valley creases around a vertex, as shown in Fig. 2. From the perspective of flat foldability, this is a natural set of variables, since flat foldability depends crucially on the arrangement of the creases around a vertex [22]. Since vertex models are well studied in statistical mechanics, we can make use of exact solutions to study flat-foldable origami CPs, in particular we make use of free-fermion models. Since we generally consider that crease assignment defects must also respect local flat-foldability requirements, we limit the vertex weights to only the set of eight weights shown in Fig. 2, except in Sec. VII, where we break Maekawa's theorem.

So-called free-fermion models are eight-vertex models which satisfy a free-fermion condition, which for the odd eight-vertex model is [53]

$$v_1 v_2 + v_3 v_4 = v_5 v_6 + v_7 v_8. \tag{3}$$

This condition allows the model to be solved via Pfaffian techniques, such as via dimer methods [60,61], which we demonstrate explicitly in Appendix A. On the homogeneous square lattice the free-fermion model is equivalent to the Ising model on the union-jack or checkerboard lattices [53]. Except for the simple square CP, the other origami CPs require staggering units, and it is unknown whether there are similar interpretations for staggered free-fermion models in terms of Ising models on a different lattice.

Since we are primarily interested in staggered lattices, we choose independent sets of vertex weights for each vertex of the two or four vertices appearing in each unit, each of which satisfies its own free-fermion condition. Except for the simple square CP, the pattern of angles around a CP's vertices causes certain vertex weights to be disallowed, with examples shown in Fig. 4. For the trapezoid CP we use two independent sets of weights v_i and w_i which satisfy

$$v_1 v_2 = v_5 v_6 + v_7 v_8, \tag{4}$$

$$w_3 w_4 = w_5 w_6 + w_7 w_8. \tag{5}$$

We are interested in the ground state being given by alternations of v_1 and w_3 with the remaining allowed vertex weights being considered defects. If we choose $v_1 = w_3 = 1$ as the ground-state weights and if we choose $v_5 = v_6 = v_7 = v_8 = y$ and $w_5 = w_6 = w_7 = w_8 = y$ for the defects which involve two

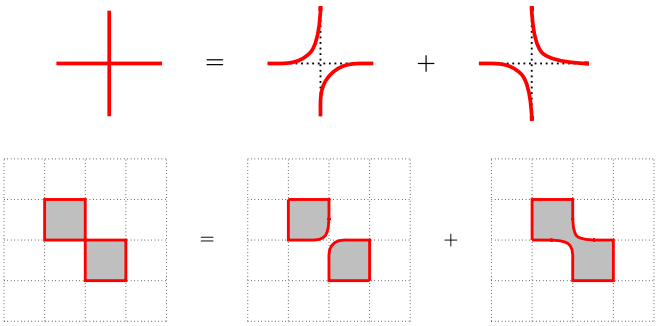

FIG. 7. Graphical interpretation of the factor of 2 in the free-fermion condition of the Miura-ori and trapezoid models. Shown on top is the interpretation around each vertex with four crease reversals and on the bottom is an example with two face-flip defects.

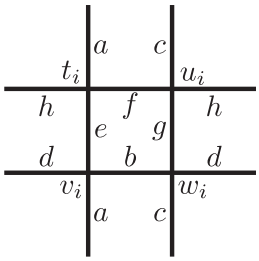

FIG. 8. Crease assignment weight notation convention on a unit of four vertices for crease weights $a, \ldots, h$, each of which represents two weights for the mountain and valley assignment separately, e.g., a_{m} and a_{v} for the a crease notation, respectively. The notation for the four vertex weights t_i, u_i, v_i, and w_i are also shown.

crease reversals (each crease is shared between two vertices, so the factor of y^2 is split between them), then we must have $v_2 = 2y^2$ and $w_4 = 2y^2$ in order to respect the free-fermion condition. The defect corresponding to reversing all four creases at a vertex then is twice as large as the naive factor of y^2 one might presume for each crease reversal. We can interpret this extra factor of 2 occurring in the fully crease-reversed vertex weights in the graphical sense, shown in Fig. 7, that each of the vertices with four crease reversals corresponds to two different arrangements of the defect loops. Therefore, the effect of imposing the free-fermion condition is to favor defects clustering together in the lattice. As long as $y < \frac{1}{2}$, defect weights v_2 and w_4 will be smaller than the other defect weights. However, as we will see below, the model has a phase transition point at $y = \sqrt{2}/2$, at which point the vertex weights which are crease reversals of the ground-state weights are equally favored, that is, $v_2 = w_4 = v_1 = w_3 = 1$. For Miura-ori CPs, similar considerations and results hold.

For Barretos's Mars CP, there are four vertex weights disallowed at each vertex and we have the free-fermion conditions

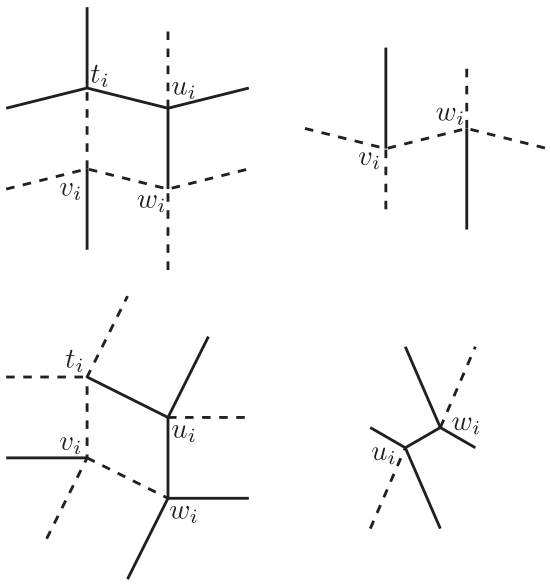

FIG. 9. From top left to bottom right, the vertex weight notation conventions for each vertex unit of Miura-ori, trapezoid, Barreto's Mars, and kite CPs.

for the four sets of vertex weights

$$v_1v_2 = v_7v_8, \quad w_3w_4 = w_7w_8, \quad t_1t_2 = t_5t_6, \quad u_3u_4 = u_5u_6 \tag{6}$$

with the ground state given by v_1, w_3 t_2, and u_4 according to Fig. 9. Again setting the ground-state weights to equal 1, we can choose defect weights given by a factor y that corresponds to the number of crease reversals at each vertex, that is, the fully crease-reversed defect weights v_2, w_4, t_1, and u_3 all equal y^2 and the remaining weights equal y. The extra factor of 2 in the fully crease-reversed weights of Miura-ori and trapezoid CPs is not present in this model.

B. Crease Boltzmann weights

The partition function of any vertex model can be modified to show explicitly the dependence of the partition function on the edge states, that is, the crease assignments; this is done by using a transformation of the vertex weights, which we now show. We define crease Boltzmann weights $a_\mathrm{m}, a_\mathrm{v}, \ldots, h_\mathrm{v}$ as shown in Fig. 8 for a general unit of four vertices, with individual weights for mountain and valley assignments of the same crease and where this is indicated by the subscript.

In order to avoid either double counting or using square roots, we use the following asymmetric transformation of the vertex weights, where for each vertex weight we add in its lower and right crease assignment dependence

$$\begin{aligned}
&v_1 \to a_\mathrm{m}b_\mathrm{v}v_1, \quad v_3 \to a_\mathrm{v}b_\mathrm{v}v_3, \quad v_5 \to a_\mathrm{v}b_\mathrm{m}v_5, \quad v_7 \to a_\mathrm{v}b_\mathrm{v}v_7,\\
&v_2 \to a_\mathrm{v}b_\mathrm{m}v_2, \quad v_4 \to a_\mathrm{m}b_\mathrm{m}v_4, \quad v_6 \to a_\mathrm{m}b_\mathrm{v}v_6, \quad v_8 \to a_\mathrm{m}b_\mathrm{m}v_8,\\
&w_1 \to c_\mathrm{m}d_\mathrm{v}w_1, \quad w_3 \to c_\mathrm{v}d_\mathrm{v}w_3, \quad w_5 \to c_\mathrm{v}d_\mathrm{m}w_5, \quad w_7 \to c_\mathrm{v}d_\mathrm{v}w_7,\\
&w_2 \to c_\mathrm{v}d_\mathrm{m}w_2, \quad w_4 \to c_\mathrm{m}d_\mathrm{m}w_4, \quad w_6 \to c_\mathrm{m}d_\mathrm{v}w_6, \quad w_8 \to c_\mathrm{m}d_\mathrm{m}w_8,\\
&t_1 \to e_\mathrm{m}f_\mathrm{v}t_1, \quad t_3 \to e_\mathrm{v}f_\mathrm{v}t_3, \quad t_5 \to e_\mathrm{v}f_\mathrm{m}t_5, \quad t_7 \to e_\mathrm{v}f_\mathrm{v}t_7,\\
&t_2 \to e_\mathrm{v}f_\mathrm{m}t_2, \quad t_4 \to e_\mathrm{m}f_\mathrm{m}t_4, \quad t_6 \to e_\mathrm{m}f_\mathrm{v}t_6, \quad t_8 \to e_\mathrm{m}f_\mathrm{m}t_8,\\
&u_1 \to g_\mathrm{m}h_\mathrm{v}u_1, \quad u_3 \to g_\mathrm{v}h_\mathrm{v}u_3, \quad u_5 \to g_\mathrm{v}h_\mathrm{m}u_5, \quad u_7 \to g_\mathrm{v}h_\mathrm{v}u_7,\\
&u_2 \to g_\mathrm{v}h_\mathrm{m}u_2, \quad u_4 \to g_\mathrm{m}h_\mathrm{m}u_4, \quad u_6 \to g_\mathrm{m}h_\mathrm{v}u_6, \quad u_8 \to g_\mathrm{m}h_\mathrm{m}u_8.
\end{aligned} \tag{7}$$

All of the odd eight-vertex results below can incorporate the extra dependence on the crease assignments after performing these transformations. We can choose the crease assignment variables corresponding to the ground-state crease configuration to all have value 1. Then as long as the remaining crease assignment variables are less than 1, the ground state will continue to be favored.

For free-fermion models, the free-fermion condition is valid identically with or without such a crease assignment dependence. For the simple square CP, Barreto's Mars, and the kite CP, the free energy can be written purely in terms of crease assignment weights, since in the free-fermion condition each of the vertex weights can be chosen to have the value $v_i = w_i = t_i = u_i = 1$. For the Miura-ori and trapezoid CPs though, the free-fermion condition cannot be satisfied in this manner, so the vertex weight dependence must continue to be explicitly shown. We show explicitly below for the simple square CP that a phase transition point can be found which depends solely on these crease assignment weights.

C. Relative local face layering Boltzmann weights

The third type of origami Boltzmann weight we consider captures the relative layer ordering of neighboring faces. We show in Sec. V below how to map from the vertex weights of the Miura-ori and the trapezoid models to the three-coloring problem on the square lattice, where each face on the square lattice is assigned one of three colors such that no two neighboring faces have the same color. The convention we define in Fig. 10 for both models shows how to assign face colors so that mountain and valley creases between two neighboring faces describes the relative layering of the two faces consistently in the lattice. We then consider color Boltzmann weights z_i for the states of each face. The exactly solvable three-coloring problem has a known phase transition point, which happens whenever all three color fugacities are equal $z_0 = z_1 = z_2$, so another phase transition point depending on the local layer ordering of faces can be established analytically, falling outside of the free-fermion model's free-fermion condition constraints.

IV. FLAT-FOLDABLE VERTEX MODELS

We now consider the origami CPs as staggered free-fermion odd eight-vertex models which have flat-foldable crease assignment defects. Using vertex weights as well as crease assignment weights, we consider their free energies as well as their critical phenomena.

A. Miura-ori CPs

For the Miura-ori four-vertex unit we use the vertex weight notation shown in Fig. 9. At each vertex, the pattern of the angles causes two vertex weights to be disallowed, so we have

$$v_3 = v_4 = t_3 = t_4 = w_1 = w_2 = u_1 = u_2 = 0. \tag{8}$$

We can use the free-fermion conditions for each independent set of vertex weights to set the ground state to be given only in terms of the weights v_1, w_3, t_2, and u_4 as discussed above. We give the fully asymmetric free energy in Appendix B.

The fully asymmetric model has phase transition points given when the following conditions hold:

$$t_1v_2w_4u_3 + v_1w_3t_2u_4 + (v_5w_6 + v_7w_8)(t_5u_6 + t_7u_8) + (v_6w_5 + v_8w_7)(t_6u_5 + t_8u_7) \pm (v_5w_7 - v_7w_5)(t_5u_7 - t_7u_5) \pm (v_6w_8 - v_8w_6)(t_6u_8 - t_8u_6) = 0, \tag{9}$$

$$t_1v_2w_4u_3 + v_1w_3t_2u_4 \pm (v_5w_7 + v_7w_5)(t_5u_7 + t_7u_5) \pm (v_6w_8 + v_8w_6)(t_6u_8 + t_8u_6) - (v_5w_6 - v_7w_8)(t_5u_6 - t_7u_8) - (v_6w_5 - v_8w_7)(t_6u_5 - t_8u_7) = 0. \tag{10}$$

There can be up to five phase transitions in this model, which are generically logarithmic of second order, although in special cases it can have two first-order phase transitions or up to three second-order phase transitions with exponent $\frac{1}{2}$ [55].

If we assume that the vertex weights t_i and u_i are given by the corresponding crease-inverted v_i and w_i weights, respectively, the free energy factorizes as an exact square and the phase transition points become more simply

$$v_1w_3 \pm v_2w_4 = 0, \tag{11}$$

$$v_1^2w_3^2 + v_2^2w_4^2 + 2(v_5w_6 + v_7w_8)(v_6w_5 + v_8w_7) - 2(v_5w_7 - v_7w_5)(v_6w_8 - v_8w_6) = 0, \tag{12}$$

$$v_1^2w_3^2 + v_2^2w_4^2 - 2(v_5w_6 - v_7w_8)(v_6w_5 - v_8w_7) + 2(v_5w_7 + v_7w_5)(v_6w_8 + v_8w_6) = 0. \tag{13}$$

If we further assume full symmetry of the weights so that the w_i weights are equal to the v_i weights rotated by 180°, the phase transition conditions become

$$v_1^2 \pm v_2^2 = 0, \tag{14}$$

$$v_1^4 + v_2^4 + 2(v_5v_8 + v_6v_7)(v_6v_7 + v_5v_8) - 2\left(v_5^2 - v_7^2\right)\left(v_6^2 - v_8^2\right) = 0, \tag{15}$$

$$v_1^4 + v_2^4 - 2(v_5v_8 - v_6v_7)(v_6v_7 - v_5v_8) + 2\left(v_5^2 + v_7^2\right)\left(v_6^2 + v_8^2\right) = 0. \tag{16}$$

If we choose $v_1 = 1$ to set the ground state and $v_5 = v_6 = v_7 = v_8 = y$ with $y < 1$, the free-fermion condition gives $v_2 = 2y^2$ and the free energy is given as

$$-\beta f_{\mathrm{Mi}} = \frac{1}{16\pi^2}\int_0^{2\pi}\int_0^{2\pi} \ln[1 + 4y^4 + 16y^8 + 4y^4(\cos\theta_1 + \cos\theta_2 - \cos\theta_1\cos\theta_2)]d\theta_1 d\theta_2. \tag{17}$$

The phase transition points then become

$$1 \pm 4y^4 = 0, \tag{18}$$

$$1 + 16y^8 + 8y^4 = 0 \tag{19}$$

and we see that there is a physical phase transition point at a positive y value

$$y_c = \sqrt{2}/2. \tag{20}$$

This point y_c corresponds to the point where the fully crease-reversed vertex weights equal the ground-state weights $v_2 = w_4 = t_1 = u_3 = 1$, although the remaining valid vertex weight defects are still less favored, less than 1, at this point.

B. Trapezoid CP

For the trapezoid two-vertex unit we use the vertex weight notation shown in Fig. 9. At each vertex, the pattern of the angles causes two vertex weights to be disallowed, so we have

$$v_1 = v_2 = w_3 = w_4 = 0. \tag{21}$$

We can use the free-fermion conditions for each independent set of vertex weights to set the ground state to be given only in terms of the weights v_3 and w_1, as discussed above. We give the free energy in Appendix B.

This model has phase transition points when the following conditions hold:

$$v_3w_1 + v_4w_2 \pm v_5w_7 \pm v_6w_8 \pm v_7w_5 \pm v_8w_6 = 0, \tag{22}$$

$$v_3w_1 + v_4w_2 \pm v_5w_7 \pm v_6w_8 \mp v_7w_5 \mp v_8w_6 = 0. \tag{23}$$

There can be up to three phase transitions of the model which are in general logarithmic of second order, although in special cases there is only one phase transition which has exponent $\frac{1}{2}$ [54].

If we assume the symmetry such that the w_i vertex weights are equal to the 180° rotated v_i weights, then the free-energy factorizes into two parts and the phase transition points are given by

$$v_1^2 + v_2^2 \pm v_5^2 \pm v_6^2 \pm v_7^2 \pm v_8^2 = 0, \tag{24}$$

$$v_1^2 + v_2^2 \pm v_5^2 \pm v_6^2 \mp v_7^2 \mp v_8^2 = 0. \tag{25}$$

If we choose $v_1 = 1$ to set the ground state and $v_5 = v_6 = v_7 = v_8 = y$ with $y < 1$, the free-fermion condition gives $v_2 = 2y^2$ and the free energy becomes

$$-\beta f_{\mathrm{T}} = \frac{1}{8\pi^2}\int_0^{2\pi}\int_0^{2\pi} \ln\{1 + 4y^4 + 2y^2[\cos\theta_2 - \cos(\theta_1 + \theta_2)]\}d\theta_1 d\theta_2. \tag{26}$$

The phase transition points then become

$$1 + 4y^4 \pm 4y^2 = 0, \tag{27}$$

$$1 + 4y^4 = 0 \tag{28}$$

and we see that there is a physical phase transition point at the positive y value

$$y_c = \sqrt{2}/2. \tag{29}$$

It can be shown that the free energy of (26) is equal to the free energy (17) of Miura-ori. In this symmetric defect case, but not in general, the two models are therefore equal. As with the Miura-ori case, y_c corresponds to the point where the fully crease-reversed vertex weights equal the ground-state weights $v_2 = w_4 = 1$, although the remaining valid vertex weight defects are still less favored, less than 1, at this point.

C. Barreto's Mars CP

For the Barreto's Mars four-vertex unit we use the vertex weight notation shown in Fig. 9. At each vertex, the pattern of the angles causes four vertex weights to be disallowed so that we have

$$t_3 = t_4 = t_7 = t_8 = u_1 = u_2 = u_7 = u_8 = 0, \tag{30}$$

$$v_3 = v_4 = v_5 = v_6 = w_1 = w_2 = w_5 = w_6 = 0. \tag{31}$$

We can use the free-fermion conditions for each independent set of vertex weights to set the ground state to be given only in terms of the weights v_7, w_8, t_5, and u_6 as discussed above. As shown in Appendix B, the free -energy is given simply by the expression

$$-\beta f_{\rm Ma} = \tfrac{1}{8}\ln[(t_1u_3v_2w_4 + t_2u_4v_1w_3 + t_5u_6v_7w_8 + t_6u_5v_8w_7)^2 - 2u_3u_4w_3w_4(t_1t_2v_1v_2 - t_5t_6v_7v_8)]. \tag{32}$$

Upon expanding, the argument of the logarithm contains only positive terms, so there is no physical phase transition point for this model. We can understand this as follows. All of the possible flat-foldable crease-reversal defects correspond to the reversal of all creases around only the diamond faces of the lattice. Since two diamond faces never share a mutual crease, all of the defects occur independently of all others; there is no interaction among the defects. Therefore, a decimation procedure could be performed for each diamond face and the resulting model would be in a frozen state.

If we rewrite the free energy with defect fugacities as

$$t_5 = u_6 = v_7 = w_8 = 1, \tag{33}$$

$$t_6 = u_5 = v_8 = w_7 = y^2, \tag{34}$$

$$t_1 = t_2 = u_3 = u_4 = v_1 = v_2 = w_3 = w_4 = y, \tag{35}$$

we have the very simple expression

$$-\beta f_{\rm Ma} = \tfrac{1}{2}\ln(1 + y^4). \tag{36}$$

This agrees with our earlier interpretation of the face-flip defects in Barreto's Mars as a noninteracting lattice gas of diamond faces. A noninteracting lattice gas with fugacity z on a lattice of size $\mathcal{N}$ will have a partition function give by

$$Z = 1 + \mathcal{N}z + \binom{\mathcal{N}}{2}z^2 + \cdots + \binom{\mathcal{N}}{\mathcal{N}}z^{\mathcal{N}} = (1+z)^{\mathcal{N}}, \tag{37}$$

with a free energy given by

$$-\beta f = \ln(1 + z). \tag{38}$$

The defect free energy of Barreto's Mars now follows, since each diamond in Barreto's Mars requires four y creases $z = y^4$ and there are $\mathcal{N}/2$ diamond faces in the lattice.

D. Kite CP

For the kite two-vertex unit we use the vertex weight notation shown in Fig. 9. At each vertex, the pattern of the angles causes four vertex weights to be disallowed, so we have

$$v_3 = v_4 = v_5 = v_6 = w_1 = w_2 = w_7 = w_8 = 0. \tag{39}$$

We can use the free-fermion conditions for each independent set of vertex weights to set the ground state to be given only in terms of the weights v_8 and w_6, as discussed above.

We give the free energy as a specialization of the four-unit column staggered odd eight-vertex free-fermion model in Appendix B, but this is unnecessary. It can be shown by considering the possible valid neighbors of each vertex weight that a given vertex weight must always be repeated on the lower-right diagonal of the weight. For a toroidal boundary condition lattice, the model is effectively a one-dimensional model. We can therefore solve it directly by a standard transfer matrix procedure and without needing to impose the free-fermion condition on the weights.

A given unit of two vertices can only have the following eight valid vertex weight combinations

$$v_1w_3, \quad v_1w_5, \quad v_8w_4, \quad v_8w_6, \quad v_2w_4, \quad v_2w_6, \quad v_7w_3, \quad v_7w_5. \tag{40}$$

We then define the following asymmetric one-dimensional transfer matrix, with rows and columns indexed by the order shown in (40):

$$T = \begin{pmatrix} v_1w_3 & 0 & 0 & v_8w_6 & & v_2w_6 & v_7w_3 & 0 \\ v_1w_3 & 0 & 0 & v_8w_6 & & v_2w_6 & v_7w_3 & 0 \\ v_1w_3 & 0 & 0 & v_8w_6 & & v_2w_6 & v_7w_3 & 0 \\ v_1w_3 & 0 & 0 & v_8w_6 & & v_2w_6 & v_7w_3 & 0 \\ 0 & v_1w_5 & v_8w_4 & 0 & v_2w_4 & 0 & 0 & v_7w_5 \\ 0 & v_1w_5 & v_8w_4 & 0 & v_2w_4 & 0 & 0 & v_7w_5 \\ 0 & v_1w_5 & v_8w_4 & 0 & v_2w_4 & 0 & 0 & v_7w_5 \\ 0 & v_1w_5 & v_8w_4 & 0 & v_2w_4 & 0 & 0 & v_7w_5 \end{pmatrix}. \tag{41}$$

The matrix T has rank 2 with nonzero eigenvalues

$$\lambda_{\pm} = \tfrac{1}{2}[v_1w_3 + v_2w_4 + v_7w_5 + v_8w_6 \pm \sqrt{D}], \tag{42}$$

where

$$\begin{aligned} D =& (v_1w_3 - v_2w_4)^2 + (v_7w_5 - v_8w_6)^2 \\ &+ 2(v_1w_3 + v_2w_4)(v_7w_5 + v_8w_6) \\ &+ 4v_1v_2w_5w_6 + 4v_7v_8w_3w_4. \end{aligned} \tag{43}$$

The partition of the one-dimensional model with N sites and periodic boundary conditions is given by

$$Z_H = \mathrm{Tr}(T^N), \tag{44}$$

so it can be written as

$$Z_H = \lambda_+^N + \lambda_-^N. \tag{45}$$

In the case of the two-dimensional lattice with toroidal boundary conditions, since each row is repeated above and below, only shifted diagonally, the partition function of the lattice with M rows is found by taking the Mth power of each of the weights which appear in the one-dimensional partition function. The quantity D cannot vanish for positive weights, so the kite model, like Barreto's Mars, does not have a phase transition.

E. Simple square CP

The simple square CP admits all eight of the odd eight-vertex weights at each vertex of the lattice. We look at the square lattice with homogeneous vertex weights, with units of two vertices as either column or bipartite staggered and with units of four vertices, column staggered. We use the vertex weight notation convention of Fig. 8.

In Appendix B we list the free energies of each of these cases except for the units of the four-vertex case, whose expression is quite large but can be found, alternatively, via a mapping of [53] from the even to the odd staggered eight-vertex model of the expressions found in [55]. All of the previous results except for the one-dimensional derivation of the kite model can be found by suitable specializations of this general free energy, although in some cases the specialization is not immediately obvious; see [54] and [55] for examples of specializations for the staggered even eight-vertex model. Therefore, the free energies of the staggered odd eight-vertex models with units of two vertices can be found more simply from the derivations in [53].

The phase transition points of the homogeneous lattice are given by the following conditions [52,53]:

$$(v_1v_2 + v_3v_4) = (v_5v_6 + v_7v_8) = 0, \tag{46}$$

$$(v_1v_3 + v_2v_4) = 0, \tag{47}$$

$$(v_5v_7 + v_6v_8) = 0, \tag{48}$$

$$\begin{aligned} &(v_1v_2 + v_3v_4)(v_5v_6 + v_7v_8) + (v_1v_3 - v_2v_4)^2 \\ &+ (v_5v_7 - v_6v_8)^2 = 0. \end{aligned} \tag{49}$$

From the phase transition point conditions, we can see that at least two of the weights must vanish for a phase transition to occur, for example, $v_1 = v_2 = 0$. The phase transitions will in general be logarithmic of second order, except in special cases where it can have an exponent of $\frac{1}{2}$ [62].

The column staggered lattice with units of two vertices has phase transitions at the points [53]

$$(v_5 + v_8)(w_6 + w_7) \pm (v_6 - v_7)(w_5 - w_8) = 0, \tag{50}$$

$$(v_6 + v_7)(w_5 + w_8) \pm (v_5 - v_8)(w_6 - w_7) = 0 \tag{51}$$

and the bipartite staggered lattice with units of two vertices has phase transitions at the points [53]

$$\begin{aligned} &- v_1w_3 - v_2w_4 + v_3w_1 + v_4w_2 + v_5w_7 + v_6w_8 \\ &\quad + v_7w_5 + v_8w_6 = 0, \\ &v_1w_3 + v_2w_4 - v_3w_1 - v_4w_2 + v_5w_7 + v_6w_8 \\ &\quad + v_7w_5 + v_8w_6 = 0, \\ &v_1w_3 + v_2w_4 + v_3w_1 + v_4w_2 - v_5w_7 - v_6w_8 \\ &\quad + v_7w_5 + v_8w_6 = 0, \\ &v_1w_3 + v_2w_4 + v_3w_1 + v_4w_2 + v_5w_7 + v_6w_8 \\ &\quad - v_7w_5 - v_8w_6 = 0. \end{aligned} \tag{52}$$

There can be up to three phase transitions of these models, which are in general logarithmic of second order, although in special cases there is only one phase transition which has exponent $\frac{1}{2}$ [54].

The expressions for the phase transition points of the general four-unit column staggered model are given by the expressions

$$-\Omega_1 + \Omega_2 + \Omega_3 + \Omega_4 = 0, \tag{53}$$

$$\Omega_1 - \Omega_2 + \Omega_3 + \Omega_4 = 0, \tag{54}$$

$$\Omega_1 + \Omega_2 - \Omega_3 + \Omega_4 = 0, \tag{55}$$

$$\Omega_1 + \Omega_2 + \Omega_3 - \Omega_4 = 0, \tag{56}$$

where

$$\begin{aligned} \Omega_1 =& t_1u_1v_2w_2 + t_2u_2v_1w_1 + t_3u_3v_4w_4 + t_4u_4v_3w_3 \\ &+ t_5u_7v_7w_5 + t_6u_8v_8w_6 + t_7u_5v_5w_7 + t_8u_6v_6w_8, \end{aligned} \tag{57}$$

$$\begin{aligned} \Omega_2 =& t_1u_1v_3w_3 + t_2u_2v_4w_4 + t_3u_3v_1w_1 + t_4u_4v_2w_2 \\ &+ t_5u_7v_5w_7 + t_6u_8v_6w_8 + t_7u_5v_7w_5 + t_8u_6v_8w_6, \end{aligned} \tag{58}$$

$$\begin{aligned} \Omega_3 =& t_1u_3v_2w_4 + t_2v_1u_4w_3 + t_3u_1v_4w_2 + t_4u_2v_3w_1 \\ &+ t_5u_6v_7w_8 + t_6u_5v_8w_7 + t_7u_8v_5w_6 + t_8u_7v_6w_5, \end{aligned} \tag{59}$$

$$\begin{aligned} \Omega_4 =& t_1u_3v_3w_1 + t_2u_4v_4w_2 + t_3u_1v_1w_3 + t_4u_2v_2w_4 \\ &+ t_5u_6v_5w_6 + t_6u_5v_6w_5 + t_7u_8v_7w_8 + t_8u_7v_8w_7. \end{aligned} \tag{60}$$

There can be up to five phase transitions in this model, which are generically logarithmic of second order, although in special cases it can have two first-order phase transitions or up to three second-order phase transitions with exponent $\frac{1}{2}$ [55].

We can also consider the general free energy as a function only of crease assignment weights, instead of vertex weights using the transformation (7), and setting all vertex weights to unity $v_i = w_i = t_i = u_i = 1$. The phase transition points are then given by the conditions

$$\pm (f_m h_m - f_v h_v)(b_m d_m - b_v d_v)(a_m c_m e_v g_v + a_v c_v e_m g_m) - (f_m h_m + f_v h_v)(b_m d_m + b_v d_v)(a_m c_v e_v g_m + a_v c_m e_m g_v)$$
$$\pm (f_m h_v - f_v h_m)(b_m d_v - b_v d_m)(a_m c_m e_m g_m + a_v c_v e_v g_v) - (f_m h_v + f_v h_m)(b_m d_v + b_v d_m)(a_m c_v e_m g_v + a_v c_m e_v g_m) = 0, \tag{61}$$

$$\pm (f_m h_m - f_v h_v)(b_m d_m - b_v d_v)(a_m c_v e_v g_m + a_v c_m e_m g_v) + (f_m h_m + f_v h_v)(b_m d_m + b_v d_v)(a_m c_m e_v g_v + a_v c_v e_m g_m)$$
$$\pm (f_m h_v - f_v h_m)(b_m d_v - b_v d_m)(a_m c_v e_m g_v + a_v c_m e_v g_m) + (f_m h_v + f_v h_m)(b_m d_v + b_v d_m)(a_m c_m e_m g_m + a_v c_v e_v g_v) = 0. \tag{62}$$

A sufficient but not necessary condition for a phase transition in these expressions is that at least four crease assignment weights are identically zero, for example, $f_m = h_v = b_m = d_m = 0$ or $a_m = c_v = e_m = g_m = 0$. We see that in general for the square lattice, phase transitions do not occur unless the symmetry of the lattice is broken.

V. FLAT-FOLDABLE THREE-COLORING MODELS

The Miura-ori and trapezoid CPs can be put into a 3-to-1 correspondence with the three-coloring model on the square lattice, as shown in Fig. 10. This was pointed out in [50] for the Miura-ori CP, although it only considers the total enumeration of colorings and not the generalization to Baxter's three-coloring problem with three-color fugacity weights z_i [56].

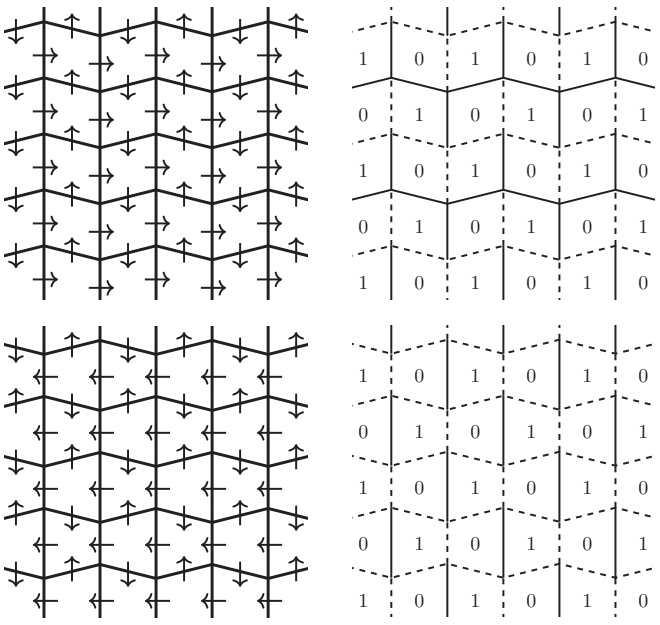

FIG. 10. Shown on the left are conventions for changing the face color across creases for the Miura-ori (top) and trapezoid (bottom) CPs. Following the arrow direction, a valley crease increases the face color number while mountain creases decrease the face color number (mod3). Shown on the right is one of the three possible color ground states the Miura-ori (top) and trapezoid (bottom) CPs map to. The other two possible ground states are found by globally increasing or decreasing all face color values by one (mod3).

Baxter's three-coloring problem on the square lattice is an exactly solved model where each face of the square lattice is allowed one of three colors with the condition that no two neighbors can share the same color. This model has a 3-to-1 mapping from the even six-vertex model [63] and can also be mapped to Baxter's symmetric even eight-vertex model [57]. It is always possible to map a staggered odd eight-vertex model to a staggered even eight-vertex model and then specialize to a homogeneous even eight-vertex model [53], for example,

$$\begin{aligned} v_1 = w_4 = \omega_5^{(e)}, \quad v_2 = w_3 = \omega_6^{(e)}, \\ v_3 = w_2 = \omega_8^{(e)}, \quad v_4 = w_1 = \omega_7^{(e)}, \\ v_5 = w_7 = \omega_1^{(e)}, \quad v_6 = w_8 = \omega_2^{(e)}, \\ v_7 = w_5 = \omega_4^{(e)}, \quad v_8 = w_6 = \omega_3^{(e)}, \end{aligned} \tag{63}$$

where the weights $\omega_i^{(e)}$ refer to the even eight-vertex model weights; see Fig. 15 for the $\omega_i^{(e)}$ notation convention. When this mapping is specialized to the even six-vertex model so that $\omega_7^{(e)} = \omega_8^{(e)} = 0$, we see that both the Miura-ori and trapezoid models have a mapping to the even six-vertex model and hence to the three-coloring problem. Alternatively, we show a direct mapping to the three-coloring problem in Fig. 10, giving a convention for how to change face colors across crease assignments [50]. We represent the colors by numbers 0, 1, 2 and we increase the color across a valley crease or decrease the color across a mountain crease in the direction of the arrows (mod3). The mapping is unique except for the initial color chosen for a face somewhere in the lattice. In Fig. 10 we show color ground states for the Miura-ori and trapezoid CPs, although two other different ground states are possible by globally increasing or decreasing all face colors by 1 (mod3).

Mapping from the three-coloring problem to the vertex models, we see that it is necessary to consider that the vertex weights come in three colors $w_{i,j}$. We then have the following mapping from color fugacity variables z_k to colored six-vertex weights $w_{i,j}$ [57]:

$$\begin{aligned} \left(\omega_{1,j}^{(e)}\right)^4 &= \left(\omega_{2,j}^{(e)}\right)^4 = (z_j)^2 z_{j-1} z_{j+1}, \\ \left(\omega_{3,j}^{(e)}\right)^4 &= z_j (z_{j-1})^2 z_{j+1}, \\ \left(\omega_{5,j}^{(e)}\right)^2 &= \left(\omega_{6,j-1}^{(e)}\right)^2 = (z_j)^2 (z_{j-1})^2, \\ \left(\omega_{4,j}^{(e)}\right)^4 &= z_j z_{j-1} (z_{j+1})^2. \end{aligned} \tag{64}$$

The three-coloring problem can also be mapped to Baxter's symmetric even eight-vertex model [57],

$$\begin{aligned}&(a^2-c^2)(b^2-d^2)=0,\quad (a^2-b^2)(c^2-d^2)=0,\\&(b^2c^2-a^2d^2)(-a^2+b^2+c^2-d^2)=(z_0z_1z_2)^2,\\&(a^2+b^2+c^2+d^2)=z_0z_1+z_1z_2+z_2z_0,\end{aligned}\tag{65}$$

where

$$\begin{aligned}&\omega_1^{(e)}=\omega_2^{(e)}=a,\quad \omega_3^{(e)}=\omega_4^{(e)}=b,\\&\omega_5^{(e)}=\omega_6^{(e)}=c,\quad \omega_7^{(e)}=\omega_8^{(e)}=d.\end{aligned}\tag{66}$$

Baxter has given the free energy of the three-coloring problem in the form [56]

$$-\beta f=\frac{1}{3}\ln(z_0z_1z_2)+\frac{1}{2}\ln\left[\frac{64(1-9t^2)^{2/3}}{27(1+t)^3(1-3t)}\right],\tag{67}$$

where t is found from

$$\frac{(1-3t^2)^3}{1-9t^2}=\frac{(z_0z_1+z_1z_2+z_2z_0)^3}{27(z_0z_1z_2)^2}\tag{68}$$

and where t is the root in the range $0\leqslant t<\frac{1}{3}$.

The face colors have a convenient origami interpretation: They give the local ordering of the layers of each face with respect to its neighbors. As discussed above, determining the global layer ordering of an origami CP, even one which is locally flat foldable, is an NP-hard problem. We see from this interpretation of the three-coloring problem, however, how to map the global flat-foldability problem to a suitable SOS model. We require, rather than three colors around a vertex, a partial ordering of the layers around each vertex and we then sum over those configurations which admit a global layer ordering, counting multiplicity. Further consideration of this type of SOS model is beyond the scope of this work.

We can see from Fig. 10 that the ground states for these models have equal numbers of two colors, so we assume without loss of generality that $z_0=z_1=1$. It can easily be seen, then, that individual face-flip defects have the effect of introducing the third color into the lattice, although in combination they can add extra one or zero colors, for example, in the middle case of the middle row of Fig. 6. The third color faces can be considered as particles with fugacity $z=z_2$, so that we can treat the model as a kind of hard square lattice gas, as discussed by Baxter [56]. In this case, we can write the pressure P as

$$P=\frac{1}{3}\ln(z)+\frac{1}{2}\ln\left[\frac{64(1-9t^2)^{2/3}}{27(1+t)^3(1-3t)}\right],\tag{69}$$

where

$$t=\begin{cases}\frac{\sqrt{2z[1+8z-\sqrt{1+12z+36z^2+32z^3}]}}{6z}, & z<1\\ \frac{\sqrt{z(z-1)}}{3z}, & z>1.\end{cases}\tag{70}$$

The three-coloring problem has a second-order phase transition with critical exponent $\frac{1}{2}$ when $z_0=z_1=z_2$, or in our defect case $z=1$ [56,63,64]. We see from the colored six-vertex mapping in (64) that this corresponds to

$$\omega_1^{(e)}=\omega_2^{(e)}=\omega_3^{(e)}=\omega_4^{(e)}=\omega_5^{(e)}=\omega_6^{(e)}\tag{71}$$

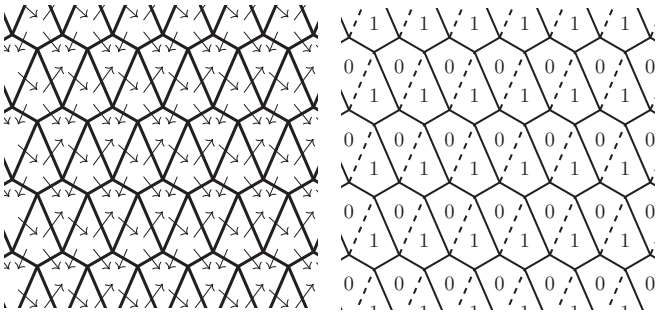

FIG. 11. Shown on the left is the convention for changing the face color across creases for the kite CP. Following the arrow direction, a valley crease increases the face color number while mountain creases decrease the face color number (mod3). Shown on the right is one of the three possible color ground states the kite model maps to. The other two possible ground states are found by globally increasing or decreasing all face color values by one (mod3).

and correspondingly

$$\begin{aligned}v_1=v_2=v_5=v_6=v_7=v_8=w_3=w_4\\=w_5=w_6=w_7=w_8,\end{aligned}\tag{72}$$

which falls outside of the free-fermion constraint for the Miura-ori and trapezoid models. Therefore, we have found an extra phase transition point of these models, which characterizes the state where all vertex weights have equal strength or, equivalently, all local layer orderings are equally probable. Above we have found phase transition points dependent on vertex weights, that is, the arrangement of creases around a vertex, as well as dependent on the crease assignments. We now also have found a phase transition dependent on the local layering of neighboring faces.

We show in Fig. 11 a mapping from the kite CP to the three-coloring problem, but since the only defects in this model are lines which traverse the entire lattice, the mapping is not surjective. It can be seen from this mapping that each line of defects causes a shift by one (mod3) of all faces below the defect line. This agrees with the demonstration above that the kite model is effectively a one-dimensional model. We note that the ground-state configuration of Barreto's Mars has a mapping to the three-coloring problem but its defects do not.

VI. LATTICE GAS OF DEFECTS

We would like to understand analytically the density of defects in these models, since the material properties of the origami tiling, such as their elastic modulus, depend on the density of defects [3]. As such, we can reinterpret these models as lattice gas models where the particles are the defects. If we choose our defect particles to be the creases themselves, we will use the variable y, in agreement with the analysis in Sec. IV. At low densities, each defect requires four creases, so it is reasonable to choose as another defect variable $z=y^{1/4}$, which at low densities also corresponds to face-flip defects. For Barreto's Mars, this correspondence at all densities is one to one, since the defects never interact with each other. However, for the other models, the correspondence is only approximate except at low densities, as can be seen in Fig. 6 and discussed

in Sec. II. For Miura-ori and trapezoid CPs, these face-flip defects behave similarly to the hard-square lattice gas, since at low densities they cannot be adjacent to each other and at high densities they form a checkerboard pattern [65–68]. For intermediate densities though, four particles can enclose a fifth one, as seen in Fig. 6, so the two models are not equal. The three-coloring defect color can also be considered as a hard particle with properties similar but not equal to hard squares [56], so we will use the notation z for both $y^{1/4}$ and the fugacity of the third color z_2 in the three-coloring problem.

As a lattice gas of defects, the partition function can then be reinterpreted as a grand canonical partition function $\mathcal{Z}$, and in the thermodynamic limit, we have the pressure P,

$$\beta P = \lim_{\mathcal{N}\to\infty} \ln(\mathcal{Z}^{1/\mathcal{N}}). \tag{73}$$

Once we rewrite the pressure in terms of the defect fugacity variables y or z, we can then find exact expressions for the density ρ of defects in the lattice, that is, the average number of defects n per site,

$$\rho = \frac{\langle n\rangle}{\mathcal{N}} = \beta z \frac{\partial P}{\partial z}. \tag{74}$$

The isothermal compressibility k_T is further given by

$$k_T = \frac{1}{\rho}\frac{\partial \rho}{\partial P} = \frac{\beta z}{\rho^2}\frac{\partial \rho}{\partial z}. \tag{75}$$

The exact free-energy results above can all be used to calculate the defect density and other thermodynamic quantities exactly. We only make use here of the symmetric defect model results from Sec. IV.

The crease defect density for Miura-ori and trapezoid CPs are equal and are given by

$$\rho_{\mathrm{Mi,Tr}}(y) = 1 - \frac{2}{\pi}\frac{\left(\frac{1}{4}-y^4\right)}{\left(\frac{1}{4}+y^4\right)} K\left(\frac{y^2}{\left(\frac{1}{4}+y^4\right)}\right) \tag{76}$$

$$= 4y^4 - 4y^8 + 16y^{12} - 36y^{16} + \cdots, \tag{77}$$

$$\rho_{\mathrm{Mi,Tr}}(z) = \frac{\rho_{\mathrm{Mi,Tr}}(y^{1/4})}{4} \tag{78}$$

$$= z - z^2 + 4z^3 - 9z^4 + \cdots, \tag{79}$$

where K is the complete elliptic integral of the first kind and the crease density of Barreto's Mars defects are given as

$$\rho_{\mathrm{Ma}}(y) = \frac{2y^4}{(1+y^4)}, \quad \rho_{\mathrm{Ma}}(z) = \frac{z}{2(1+z)}. \tag{80}$$

The layer order defect densities for Miura-ori and trapezoid CPs are large algebraic expressions but can be found through a straightforward application of (74) to the expressions (69) and (70) in Sec. V.

Miura-ori and trapezoid CPs have a phase transition point at $y_c = \sqrt{2}/2$ and $z_c = \frac{1}{4}$, where $\rho(y_c) = 1$ and $\rho(z_c) = \frac{1}{4}$, respectively; Barreto's Mars does not have a phase transition. In all cases the densities approach $\rho \to 2$ as $y \to \infty$ and $\rho \to \frac{1}{2}$ as $z \to \infty$. We plot in Fig. 12 the densities of each case.

For low crease-reversal defect fugacities of the Miura-ori and trapezoid models, the density behaves as a quartic up to near the phase transition point, as can be seen in the plot in Fig. 12(b) where the density is almost linear in z up to z_c.

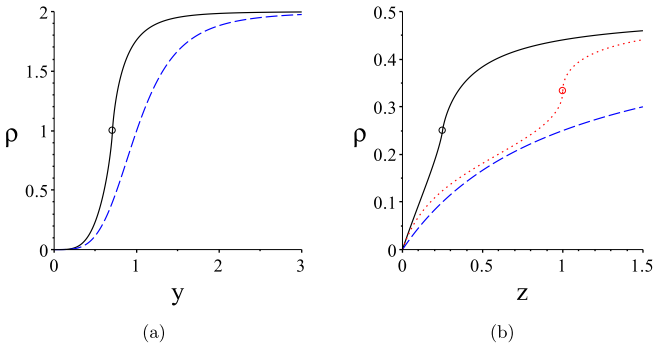

FIG. 12. Comparison of the crease-reversal defect densities as a function of (a) y and (b) z for Miura-ori and trapezoid CPs (solid black line) and Barreto's Mars CPs (blue dashed line). Also shown in (b) is the Miura-ori and trapezoid layer defect density as a function of layer defects z (dotted red line). Phase transition points are indicated by circles.

The Barreto's Mars defect density is always smaller than the corresponding density for the Miura-ori and trapezoid models for the same fugacity variable, showing that it is more stable against defects. Conversely, the defect density of the Miura-ori and trapezoid models is more easily tunable. As a function of layer ordering defects, the Miura-ori and trapezoid's density does not agree with their density as a function of crease defects except only at very low and very high densities and otherwise has a more complex behavior, with a phase transition at $z_c = 1$ where $\rho(z_c) = 1/3$. Since the phase transition in the three-coloring problem happens for a larger value of z than the phase transition as a function of creases, we see that the long-range crease order disappears before the long-range layering order in the lattice. Therefore, to the extent that mechanical properties depend on the layering order versus the crease order, these origami CPs are more stable and tunable for a larger range of defect densities.

We note also that at defect saturation $y, z \to \infty$, the CP is totally crease reversed and folds in an orderly fashion like the ground-state folding, though reversed. Therefore, the points $\rho(y) = 1$ and $\rho(z) = \frac{1}{4}$ seem to represent states of maximal folding disorder and we see that the crease defect phase transition points at $y_c = \sqrt{2}/2$ and $z_c = \frac{1}{4}$ exactly correspond to these points. The layer defect phase transition point at $z_c = 1$, interestingly, is at a higher defect density, corresponding to 2/3 of the defect saturation.

The isothermal compressibility k_{T} is proportional to the derivative of the density

$$\frac{d\rho_{\mathrm{Mi,Tr}}(y)}{dy} = \frac{4}{\pi y}\left[K\left(\frac{y^2}{\left(\frac{1}{4}+y^4\right)}\right) - E\left(\frac{y^2}{\left(\frac{1}{4}+y^4\right)}\right)\right], \tag{81}$$

$$\frac{d\rho_{\mathrm{Mi,Tr}}(z)}{dz} = \frac{1}{4\pi z}\left[K\left(\frac{z^{1/2}}{\left(\frac{1}{4}+z\right)}\right) - E\left(\frac{z^{1/2}}{\left(\frac{1}{4}+z\right)}\right)\right], \tag{82}$$

where E is the complete elliptic integral of the second kind, and

$$\frac{d\rho_{\mathrm{Ma}}(y)}{dy} = \frac{8y^3}{(1+y^4)^2}, \quad \frac{d\rho_{\mathrm{Ma}}(z)}{dy} = \frac{1}{2(1+z)^2}. \tag{83}$$

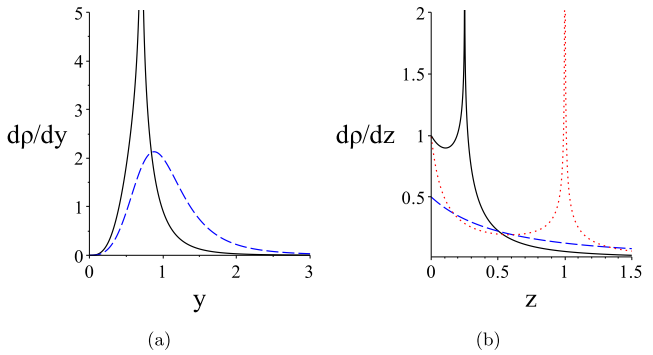

FIG. 13. Comparison of the derivative of the crease-reversal defect density as a function of (a) y and (b) z for Miura-ori and trapezoid CPs (solid black line) and Barreto's Mars CPs (blue dashed line). Also shown in (b) is the Miura-ori and trapezoid layer defect density derivative as a function of layer defects z (dotted red line).

Again, expressions for Miura-ori and trapezoid CPs as a function of the layer defect fugacity z can be found in a straightforward fashion. We plot in Fig. 13 the derivative of the densities as a function of both crease-reversal defect fugacities y and z and layer defect fugacity z. In Fig. 14 we further compute the equation of state of these models.

VII. SIMPLE SQUARE CP WITH MAEKAWA DEFECTS

As a final investigation we can consider breaking Maekawa's theorem at each vertex of the homogeneous simple square CP; the model will no longer be locally flat foldable. This opens up eight more possible vertex configurations, the even eight-vertex weights $\omega_i^{(e)}$ shown in Fig. 15, for a total of 16 weights in the model. This is the 16-vertex model [53].

There are few exactly solvable known cases of the general 16-vertex model. The only known cases with all nonzero weights are Baxter's symmetric even eight-vertex model [59,63,64], the even and odd free-fermion models mapped via the weak-graph expansion transformation [52,53,59], and Deguchi's model [69]. Of these, the only solvable case with all positive weights is the 16-vertex representation of the even free-fermion eight-vertex model [59], which has weights in the symmetric form

$$\omega_{2i}^{(e)} = \omega_{2i-1}^{(e)}, \quad v_{2i} = v_{2i-1}, \quad i = 1, \ldots, 8 \tag{84}$$

$$\omega_1^{(e)}\omega_3^{(e)} + \omega_5^{(e)}\omega_7^{(e)} = v_1 v_3 + v_5 v_7, \tag{85}$$

where this second condition is the 16-vertex model's representation of the free-fermion condition. This model has a mapping via a weak-graph transformation [53] to the even free-fermion eight-vertex model with weights $\tilde{w}_i$, given by

$$\tilde{w}_1 = \tfrac{1}{2}\big(\omega_1^{(e)} + \omega_3^{(e)} + \omega_5^{(e)} + \omega_7^{(e)} + v_1 + v_3 + v_5 + v_7\big), \tag{86}$$

$$\tilde{w}_2 = \tfrac{1}{2}\big(\omega_1^{(e)} + \omega_3^{(e)} + \omega_5^{(e)} + \omega_7^{(e)} - v_1 - v_3 - v_5 - v_7\big), \tag{87}$$

$$\tilde{w}_3 = \tfrac{1}{2}\big(\omega_1^{(e)} + \omega_3^{(e)} - \omega_5^{(e)} - \omega_7^{(e)} - v_1 - v_3 + v_5 + v_7\big), \tag{88}$$

$$\tilde{w}_4 = \tfrac{1}{2}\big(\omega_1^{(e)} + \omega_3^{(e)} - \omega_5^{(e)} - \omega_7^{(e)} + v_1 + v_3 - v_5 - v_7\big), \tag{89}$$

$$\tilde{w}_5 = \tfrac{1}{2}\big(\omega_1^{(e)} - \omega_3^{(e)} + \omega_5^{(e)} - \omega_7^{(e)} - v_1 + v_3 + v_5 - v_7\big), \tag{90}$$

$$\tilde{w}_6 = \tfrac{1}{2}\big(\omega_1^{(e)} - \omega_3^{(e)} + \omega_5^{(e)} - \omega_7^{(e)} + v_1 - v_3 - v_5 + v_7\big), \tag{91}$$

$$\tilde{w}_7 = \tfrac{1}{2}\big(\omega_1^{(e)} - \omega_3^{(e)} - \omega_5^{(e)} + \omega_7^{(e)} - v_1 + v_3 - v_5 + v_7\big), \tag{92}$$

$$\tilde{w}_8 = \tfrac{1}{2}\big(\omega_1^{(e)} - \omega_3^{(e)} - \omega_5^{(e)} + \omega_7^{(e)} + v_1 - v_3 + v_5 - v_7\big). \tag{93}$$

The exact solution of the even free-fermion eight-vertex model has the free energy [62]

$$-\beta f = \frac{1}{8\pi^2}\int_0^{2\pi}\int_0^{2\pi} d\theta_1 d\theta_2 \ln(A + 2B\cos(\theta_1) + 2C\cos(\theta_2) + 2D\cos(\theta_1 - \theta_2) + 2E\cos(\theta_1 + \theta_2), \tag{94}$$

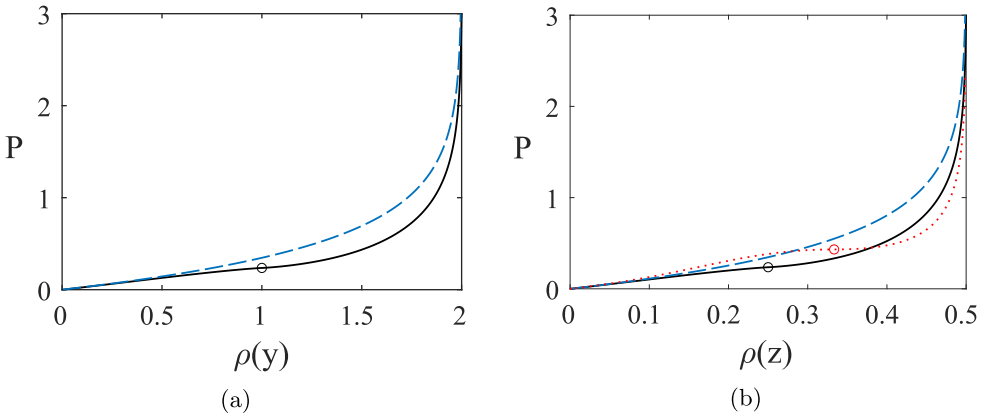

FIG. 14. Equations of state as a function of crease-reversal densities (a) $\rho(y)$ and (b) $\rho(z)$ for Miura-ori and trapezoid CPs (solid black line) and Barreto's Mars CPs (blue dashed line). Also shown in (b) is the Miura-ori and trapezoid equation of state as a function of layer defect density $\rho(z)$ (dotted red line). Phase transition points are indicated by circles.

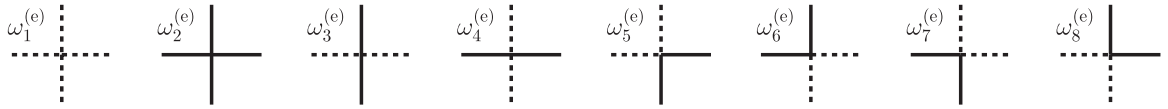

FIG. 15. Even eight-vertex model weights, with bond states shown in terms of line type, dashed or solid.

where

$$A = \tilde{w}_1^2 + \tilde{w}_2^2 + \tilde{w}_3^2 + \tilde{w}_4^2, \tag{95}$$

$$B = \tilde{w}_1\tilde{w}_3 - \tilde{w}_2\tilde{w}_4, \tag{96}$$

$$C = \tilde{w}_1\tilde{w}_4 - \tilde{w}_2\tilde{w}_3, \tag{97}$$

$$D = \tilde{w}_3\tilde{w}_4 - \tilde{w}_7\tilde{w}_8 = \tilde{w}_5\tilde{w}_6 - \tilde{w}_1\tilde{w}_2, \tag{98}$$

$$E = \tilde{w}_3\tilde{w}_4 - \tilde{w}_5\tilde{w}_6 = \tilde{w}_7\tilde{w}_8 - \tilde{w}_1\tilde{w}_2, \tag{99}$$

which has phase transitions at the points given by each of the following conditions, expressed in terms of the 16-vertex model weights $\omega_i^{(e)}$ and v_i:

$$\omega_1^{(e)} + \omega_3^{(e)} = \omega_5^{(e)} + \omega_7^{(e)} + v_1 + v_3 + v_5 + v_7, \tag{100}$$

$$\omega_5^{(e)} + \omega_7^{(e)} = \omega_1^{(e)} + \omega_3^{(e)} + v_1 + v_3 + v_5 + v_7, \tag{101}$$

$$v_1 + v_3 = \omega_1^{(e)} + \omega_3^{(e)} + \omega_5^{(e)} + \omega_7^{(e)} + v_5 + v_7, \tag{102}$$

$$v_5 + v_7 = \omega_1^{(e)} + \omega_3^{(e)} + \omega_5^{(e)} + \omega_7^{(e)} + v_1 + v_3. \tag{103}$$

These phase transitions are second-order logarithmic phase transitions in general, except in certain subcases where they are second order with critical exponent $\frac{1}{2}$ [62].

If we choose all Maekawa defects to have equal weights so that $\omega_i^{(e)} = \omega$, then the free-fermion condition becomes

$$2\omega^2 = v_1v_3 + v_5v_7. \tag{104}$$

The free-fermion condition (104) shows that this solvable case requires Maekawa defects to have Boltzmann weights $\omega_i^{(e)}$ of the same order as the flat-foldable weights v_i, which may not be a suitable assumption for certain applications, and it is not a simple extension of the flat-foldable model considered earlier in Sec. IV E. Its phase transitions occur at

$$v_1 + v_3 = 4\omega + v_5 + v_7, \tag{105}$$

$$v_5 + v_7 = 4\omega + v_1 + v_3. \tag{106}$$

VIII. DISCUSSION

A. Rigid foldability

In this paper we have concentrated on local flat-foldability properties of origami CPs. A further interest in the study of origami CPs is the determination of their rigid foldability [7,19,23,70–73], where as long as the hinges move, the faces are not require to bend for the lattice to fold. The Miura-ori, Barreto's Mars, trapezoid, and kite CPs are rigidly foldable in their ground states [23]. It can be proven that the defects break rigid foldability, using known relations between crease assignments and fold angles for degree 4 vertices [74]. In practice, this may not present an issue. Indeed, an origami triangular lattice tessellation in [13] with 198 creases of size 333 μm was able to self-fold correctly while requiring face bending to achieve the final state. Therefore, it would be beneficial to also model the face bending properties of these models [12]. Using a triangular or union-jack lattice from which to construct staggered free-fermion odd eight-vertex models, it would be possible to model some face bending properties. In [3] the authors showed how defects create subtle diagonal creases along neighboring faces, which a triangular lattice can easily capture. Otherwise, the two states of the diagonal bond can represent a concave or a convex face curvature. Using a union-jack lattice, each face of the origami CP is now covered with four creases which meet at a vertex. The two states of each bond in the face can then be used to model various degrees of curvature of the face.

B. Free-fermion models

Most of the exactly solvable models used in this work were free-fermion models. The homogeneous free-fermion model, used to model the homogeneous simple square CP as well as the Maekawa defects case, is equivalent to the union-jack and checkerboard lattice Ising models, and its phase transitions can all be mapped to the triangular lattice Ising model [53]. It is unknown whether staggered free-fermion eight-vertex models also have similar interpretations in terms of Ising models on larger or modified lattices. In principle, the correlation functions of all free-fermion models can be studied in a straightforward manner by generalizing the methods in [75], but as far as we are aware this has not yet been carried out for any of the cases of interest in this work.

C. Finite lattice results

We have focused in this work on the thermodynamic limit, since it is only in this limit that phase transitions arise and can be analyzed. However, finite lattice partition functions are of interest in any experimental implementation of these origami CPs. Free-fermion model partition functions can be solved exactly on the finite lattice, in particular on the finite torus, using the methods in [60,61]. This may be of interest in practical applications, since toroidal boundary conditions become a better approximation to free boundary conditions as the size of the lattice increases. In fact, for large enough lattice sizes the thermodynamic limit results may be a very good approximation of the properties of finite free boundary origami lattices.

D. Random crumpling

Various previous studies have considered random crumplings on lattices (see [45–47] for reviews), but they have generally neglected to distinguish between mountain and

valley folds and did not incorporate Maekawa's theorem at each vertex; they also did not use exactly solvable models. It would be interesting to seek an exact solution of these problems. In order to model random lattice crumpling problems, three-state bond variables are necessary, one for the absence of a crease and two for mountain and valley creases, and it is necessary to disallow sudden corner bends of creases. Also, higher degree vertices are preferable, since they can model more crease angles in the lattice. Three-state vertex models, such as the 19-vertex Izergin-Korepin model [76], are well known, although the only known exactly solvable models are for the square lattice, and their symmetries do not allow the exclusion of corner bends of creases, which locally break Kawasaki's theorem and hence are not locally flat foldable, without destroying the integrability of the model.

IX. CONCLUSION

We have made extensive use of exactly solvable models in order to study phase transition points of origami CP models. We have found phase transitions which depend on the arrangement of crease assignments around a vertex, on individual crease assignments, as well as on the local layer ordering of neighboring faces in the lattice. We also have found a phase transition in the case of breaking Maekawa's theorem at each vertex, so the model is no longer locally flat foldable.

Using our exactly solvable models, we have interpreted the flat-foldable crease-reversal and local layering order defects in terms of a lattice gas, which allowed us to find exact analytic expressions for their density as a function of the defect fugacity variables. This has allowed us to characterize how stable different CPs are against flat-foldable defects or, conversely, how tunable the origami CP is for the setting of the defect density. Miura-ori and trapezoid CPs have the same defect density dependence which is less stable, and therefore more tunable, than Barreto's Mars CP.

We have found that Miura-ori and trapezoid CPs have phase transition points which determine either the loss of long-range crease order in the lattice or else the loss of long-range layer ordering in the lattice. Since the phase transition point depending on layer ordering is at a greater fugacity location compared to crease order, we see that any mechanical properties depending on layering order has a broader range of tunability compared to mechanical properties depending on crease ordering in the lattice. Barreto's Mars CP does not have a crease order phase transition point, and though it is more stable against defects, defects can continue to be added until saturation without destroying the long-range crease order properties of the CP. The simple square CP has a crease order phase transition point as long as the vertex weights or edge crease weights are sufficiently anisotropic; furthermore, its free energy, and hence its phase transition point, can be written purely in terms of crease edge variables. Barreto's Mars and the simple square CPs do not feature a three-coloring problem interpretation and so we were not able to analyze the layer ordering properties of these models. The kite CP is effectively a one-dimensional model whose defects are lines which traverse the entire lattice, making it extremely stable; consequently, it does not have a phase transition point. It remains to confirm experimentally the conclusions of this paper.

ACKNOWLEDGMENTS

We gratefully acknowledge numerous helpful conversations with Arthur A. Evans, as well as with Nathan Clisby and Iwan Jensen, during the preparation of this work. We also thank Robert J. Lang for a careful reading of the manuscript and helpful suggestions. We would like to thank the Australian Research Council for supporting this work under the Discovery Project scheme (Project No. DP140101110).

APPENDIX A: DIMER MODEL SOLUTION OF THE FOUR-STAGGERED ODD EIGHT-VERTEX MODEL

In this appendix we outline the dimer solution method of [60,61], generalizing the construction in [53] to construct the free energy of the odd eight-vertex four-unit staggered free-fermion models. We consider a square lattice with toroidal boundary conditions of size $M \times N$ and use the dimer construction of [53], shown in Fig. 16. Each of the vertex weights can be written in terms of the lattice bond weights z_i, defined in Fig. 17.

From Figs. 16 and 17, the odd eight-vertex weights v_i have the following expressions in terms of lattice bond weights z_i:

$$v_1 = z_1 z_8 + z_3 z_7, \quad v_2 = z_6, \quad v_3 = z_2 z_7 + z_4 z_8, \quad v_4 = z_5, \tag{A1}$$

$$v_5 = z_1 z_6 + z_4 z_5, \quad v_6 = z_8, \quad v_7 = z_2 z_5 + z_3 z_6, \quad v_8 = z_7. \tag{A2}$$

It can be seen from these relations that the vertex weights v_i follow the free-fermion condition

$$v_1 v_2 + v_3 v_4 = v_5 v_6 + v_7 v_8. \tag{A3}$$

One of the weights z_i is superfluous and can be made arbitrary. We here take $z_2 = 1$. Solving for the bond weights z_i in terms of the vertex weights v_i, we have

$$z_1 = \frac{v_4 v_8 + v_5 v_6 - v_3 v_4}{v_2 v_6} = \frac{v_1 v_2 + v_4 v_8 - v_7 v_8}{v_2 v_6}, \tag{A4}$$

$$z_2 = 1, \quad z_3 = \frac{v_7 - v_4}{v_2}, \quad z_4 = \frac{v_3 - v_8}{v_6}, \tag{A5}$$

$$z_5 = v_4, \quad z_6 = v_2, \quad z_7 = v_8, \quad z_8 = v_6. \tag{A6}$$

For the four-unit staggered odd eight-vertex free-fermion model, we define independent vertex weights on each of the four cluster units. We show in Fig. 17 the numbering convention for each cluster. From the first to the fourth we use the vertex weight notations v_i, w_i, t_i, and u_i, respectively. Each independent set of vertex weights satisfies the free-fermion constraint.

We use a straightforward column staggering of the four units on the lattice. The model's partition function is given by a Pfaffian whose square is given by the determinant of the matrix

$$M_{4U} = T \otimes I_N \otimes I_M + A_1 \otimes H_N^{\mathrm{T}} \otimes I_M + A_2 \otimes H_N \otimes I_M + B_1 \otimes I_N \otimes H_M^{\mathrm{T}} + B_2 \otimes I_N \otimes H_M, \tag{A7}$$

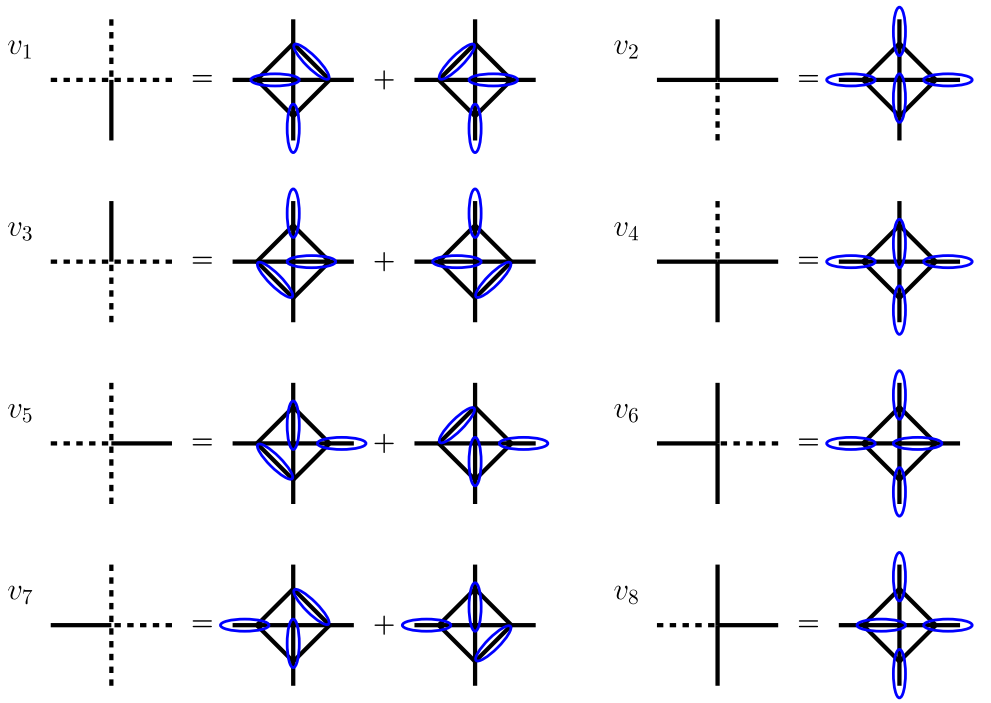

FIG. 16. Correspondence between the odd eight-vertex model weights and dimer coverings.

where the I_n are $n \times n$ identity matrices, where the $n \times n$ matrix H_n is defined as

$$H_n = \begin{pmatrix} 0 & 1 & 0 & \cdots & 0 \\ 0 & 0 & 1 & \cdots & 0 \\ \vdots & \vdots & \vdots & \ddots & \vdots \\ 0 & 0 & 0 & \cdots & 1 \\ 1 & 0 & 0 & \cdots & 0 \end{pmatrix}, \tag{A8}$$

where the 20×20 matrix T is defined as

$$T = \begin{pmatrix} T_1 & 0 & 0 & 0 \\ 0 & T_2 & 0 & 0 \\ 0 & 0 & T_3 & 0 \\ 0 & 0 & 0 & T_4 \end{pmatrix}, \tag{A9}$$

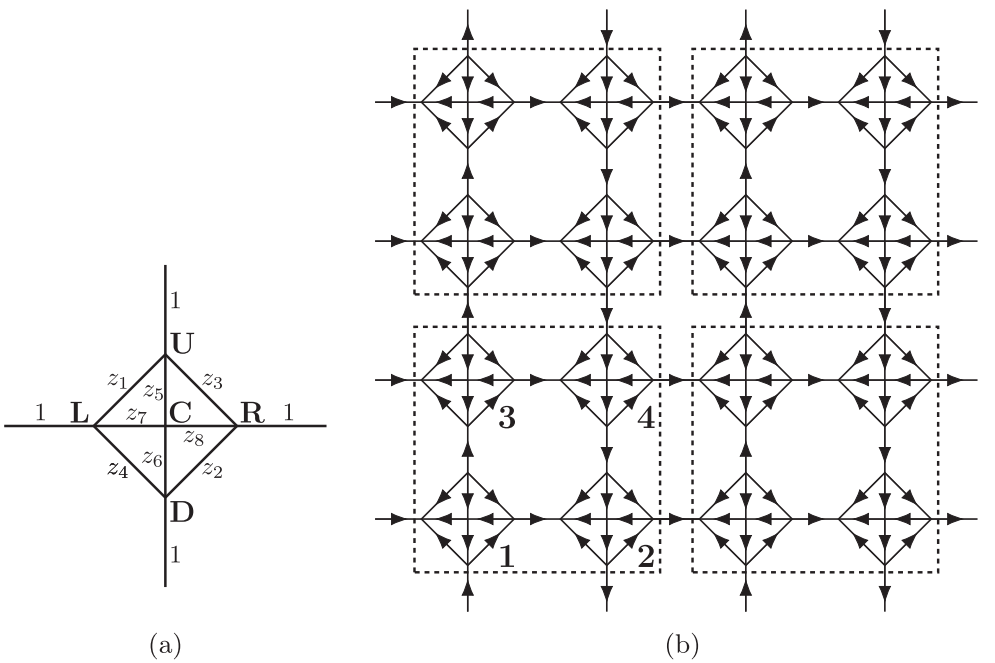

FIG. 17. (a) Vertex and bond weight definitions around a cluster for the odd eight-vertex model. (b) Orientation graph convention on a column staggered lattice with four dimer cluster units for the odd eight-vertex model. The numbering convention for each of the four cluster units is shown.

where T_i are defined as

$$T_i = \begin{array}{c} \\ U_i \\ D_i \\ L_i \\ R_i \\ C_i \end{array} \begin{array}{c} \begin{array}{ccccc} U_i & D_i & L_i & R_i & C_i \end{array} \\ \begin{pmatrix} 0 & * & z_1 & z_3 & z_5 \\ * & 0 & z_4 & z_2 & -z_6 \\ -z_1 & -z_4 & 0 & * & -z_7 \\ -z_3 & -z_2 & * & 0 & z_8 \\ -z_5 & z_6 & z_7 & -z_8 & 0 \end{pmatrix} \end{array}, \tag{A10}$$

with the appropriate independent unit vertex weights substituted for the bond weights z_i in each T_i and where the notation $*$ represents 0 except for the particular T elements

$$(T)_{U_1,D_3} = -(T)_{D_3,U_1} = 1, \tag{A11}$$

$$(T)_{R_1,L_2} = -(T)_{L_2,R_1} = 1, \tag{A12}$$

$$(T)_{U_2,D_4} = -(T)_{D_4,U_2} = -1, \tag{A13}$$

$$(T)_{R_3,L_4} = -(T)_{L_4,R_3} = 1 \tag{A14}$$

and where the nonzero elements of the 20×20 matrices A_1, A_2, B_1, and B_2 are given by

$$(A_1)_{D_1,U_3} = -(A_1)_{D_2,U_4} = -1, \tag{A15}$$

$$(A_2)_{U_3,D_1} = -(A_2)_{U_4,D_2} = 1, \tag{A16}$$

$$(B_1)_{L_1,R_2} = (B_1)_{L_3,R_4} = -1, \tag{A17}$$

$$(B_2)_{R_2,L_1} = (B_2)_{R_4,L_3} = 1. \tag{A18}$$

The matrices H_n have eigenvalues $e^{2\pi ik/n}$, and since the H_n are unitary,

$$H_n H_n^{\mathrm{T}} = 1, \tag{A19}$$

so the eigenvalues of H_n^{T} are $e^{-2\pi ik/n}$. The determinant of $M_{4\mathrm{U}}$ is then given by the double product of the determinant $D(\theta_1, \theta_2)$,

$$\mathrm{Det}(M_{4\mathrm{U}}) = \prod_{\theta_1} \prod_{\theta_2} D(\theta_1, \theta_2), \tag{A20}$$

where $D(\theta_1, \theta_2)$ is the determinant of the matrix T with additional entries coming from the diagonalization of the matrices A_1, A_2, B_1, and B_2,

$$(T)_{D_1,U_3} = -(T)_{D_2,U_4} = -e^{-i\theta_1}, \tag{A21}$$

$$(T)_{U_3,D_1} = -(T)_{U_4,D_2} = e^{i\theta_1}, \tag{A22}$$

$$(T)_{L_1,R_2} = (T)_{L_3,R_4} = -e^{-i\theta_2}, \tag{A23}$$

$$(T)_{R_2,L_1} = (T)_{R_4,L_3} = e^{i\theta_2}, \tag{A24}$$

where

$$\theta_1 = \frac{2\pi n}{N}, \quad \theta_2 = \frac{2\pi m}{M} \tag{A25}$$

with $n = 1, \ldots, N$ and $m = 1, \ldots, M$.

The partition function $Z_{4\mathrm{U}}$ is the square root of the determinant of $M_{4\mathrm{U}}$.[1] In the thermodynamic limit, the free energy $f_{4\mathrm{U}}$ is given by

$$f_{4\mathrm{U}} = -\frac{1}{4\beta} \lim_{M\to\infty} \lim_{N\to\infty} \frac{1}{MN} \ln Z_{4\mathrm{U}} \tag{A26}$$

$$= -\frac{1}{4\beta} \lim_{M\to\infty} \lim_{N\to\infty} \frac{1}{MN} \ln \mathrm{Det}(M_{4\mathrm{U}})^{1/2}, \tag{A27}$$

where the leading factor of 4 is due to the fact that there are four dimer clusters in each unit.

The logarithm of the products in the determinant can be expanded and written as integrals in the thermodynamic limit, giving the free-energy expression

$$-\beta f_{4\mathrm{U}} = \frac{1}{32\pi^2} \int_0^{2\pi} \int_0^{2\pi} \ln[D(\theta_1, \theta_2)] d\theta_1 d\theta_2. \tag{A28}$$

The expression for the free energy is of the form

$$\begin{aligned} -\beta f_{4\mathrm{U}} = \frac{1}{32\pi^2} \int_0^{2\pi} \int_0^{2\pi} & \ln[A + 2B\cos(\theta_1) + 2C\cos(\theta_2) + 2D\cos(\theta_1+\theta_2) + 2E\cos(\theta_1-\theta_2) + 2F\cos(2\theta_1) \\ & + 2G\cos(2\theta_2) + 2H\cos(2\theta_1+\theta_2) + 2I\cos(2\theta_1-\theta_2) + 2J\cos(\theta_1+2\theta_2) + 2K\cos(\theta_1-2\theta_2) \\ & + 2L\cos(2\theta_1+2\theta_2) + 2M\cos(2\theta_1-2\theta_2)] d\theta_1 d\theta_2, \end{aligned} \tag{A29}$$

where the $A, \ldots, M$ are large polynomials in the four sets of vertex weights t_i, u_i, v_i, and w_i.

Four phase transition conditions can be found by setting $\theta_1, \theta_2 = 0, \pi$ in $D(\theta_1, \theta_2)$, as explained in [77,78]. A phase transition occurs when at least one of the four conditions is satisfied, and each of the conditions can define multiple phase transition points [54,55,79,80]. For the homogeneous lattice, that is, the unstaggered lattice, it can be proven that all of the physical phase transitions can be found from such conditions [77,78]. For the staggered lattices we are considering, it appears that no such proof is known however.

[1] On the finite lattice, for toroidal boundary conditions, four Pfaffians are actually needed, but they become degenerate in the thermodynamic limit [60,61].

APPENDIX B: FREE ENERGIES

Here we collect particular free-energy expressions. The expressions for the general four-unit staggered model are very large and we omit them. Using the mappings between the staggered even eight-vertex models and staggered odd eight-vertex models of [53], the expressions in [55] can alternatively be used for the free energy of this most general case.

1. Miura free energy

The expression for the Miura free energy is of the form (A29), where after simplifications of the general terms using the free-fermion conditions for the four sets of vertex weights we have the following expressions for each term:

$$\begin{aligned}A =& u_3^2v_2^2w_4^2t_1^2 + t_2^2u_4^2w_3^2v_1^2 + 2t_1t_2v_1v_2u_3u_4w_3w_4 + 2t_5t_6u_5u_6v_7v_8w_7w_8 + 2t_7t_8u_7u_8v_5v_6w_5w_6 + \left(v_5^2w_6^2 + v_7^2w_8^2\right)\\ &\times \left(t_5^2u_6^2 + t_7^2u_8^2\right) + \left(v_5^2w_7^2 + v_7^2w_5^2\right)\left(t_5^2u_7^2 + t_7^2u_5^2\right) + \left(v_6^2w_5^2 + v_8^2w_7^2\right)\left(t_6^2u_5^2 + t_8^2u_7^2\right) + \left(v_6^2w_8^2 + v_8^2w_6^2\right)\left(t_6^2u_8^2 + t_8^2u_6^2\right)\\ &+ 2(t_7u_5v_5w_7 + t_8u_6v_6w_8)(t_5u_7v_7w_5 + t_6u_8v_8w_6) + 2(t_7u_8v_7w_8 + t_8u_7v_8w_7)(t_5u_6v_5w_6 + t_6u_5v_6w_5)\\ &+ 2(t_1u_3v_2w_4 + t_2u_4v_1w_3)(t_5u_6v_7w_8 + t_6u_5v_8w_7 + t_7u_8v_5w_6 + t_8u_7v_6w_5),\end{aligned} \tag{B1}$$

$$\begin{aligned}B =& \left(-v_5^2w_6w_7 + v_7^2w_5w_8\right)\left(t_5^2u_6u_7 - t_7^2u_5u_8\right) + \left(-v_5v_8w_6^2 + v_6v_7w_8^2\right)\left(t_5t_8u_6^2 - t_6t_7u_8^2\right)\\ &+ \left(-v_5v_8w_7^2 + v_6v_7w_5^2\right)\left(t_5t_8u_7^2 - t_6t_7u_5^2\right) + \left(v_6^2w_5w_8 - v_8^2w_6w_7\right)\left(-t_6^2u_5u_8 + t_8^2u_6u_7\right)\\ &+ (t_1u_3v_2w_4 + t_2u_4v_1w_3)(t_5u_7v_7w_5 + t_6u_8v_8w_6 + t_7u_5v_5w_7 + t_8u_6v_6w_8)\\ &+ (u_5u_7w_5w_7 + u_6u_8w_6w_8)(t_5t_6v_7v_8 + t_7t_8v_5v_6) + (u_5u_6w_7w_8 + u_7u_8w_5w_6)(t_5t_7v_5v_7 + t_6t_8v_6v_8)\end{aligned} \tag{B2}$$

$$\begin{aligned}C =& \left(-u_6^2w_6w_8 + u_7^2w_5w_7\right)\left(-t_5^2v_5v_7 + t_8^2v_6v_8\right) + \left(u_5^2w_5w_7 - u_8^2w_6w_8\right)\left(t_6^2v_6v_8 - t_7^2v_5v_7\right)\\ &- u_5u_7\left[t_5t_7\left(v_5^2w_7^2 + v_7^2w_5^2\right) - t_6t_8\left(v_6^2w_5^2 + v_8^2w_7^2\right)\right] + u_6u_8\left[t_5t_7\left(v_5^2w_6^2 + v_7^2w_8^2\right) - t_6t_8\left(v_6^2w_8^2 + v_8^2w_6^2\right)\right]\\ &+ (v_5v_8w_6w_7 + v_6v_7w_5w_8)(t_5t_6u_5u_6 + t_7t_8u_7u_8) + (v_5v_6w_5w_6 + v_7v_8w_7w_8)(t_5t_8u_6u_7 + t_6t_7u_5u_8)\\ &+ (t_1u_3v_2w_4 + t_2u_4v_1w_3)(t_5u_6v_5w_6 + t_6u_5v_6w_5 + t_7u_8v_7w_8 + t_8u_7v_8w_7),\end{aligned} \tag{B3}$$

$$\begin{aligned}D =& \left[t_7\left(-v_5^2w_6w_7 + v_7^2w_5w_8\right)t_5 - t_6t_8\left(v_6^2w_5w_8 - v_8^2w_6w_7\right)\right]u_7u_8 - \left[u_8\left(t_6^2v_6v_8 - t_7^2v_5v_7\right)u_5 + u_6u_7\left(t_5^2v_5v_7 - t_8^2v_6v_8\right)\right]w_7w_8\\ &\times \left[-u_7\left(v_5v_8w_7^2 - v_6v_7w_5^2\right)u_5 + u_6u_8\left(v_5v_8w_6^2 - v_6v_7w_8^2\right)\right]t_6t_5 - \left[t_8\left(-u_6^2w_6w_8 + u_7^2w_5w_7\right)t_5\right.\\ &\left.- t_6t_7\left(u_5^2w_5w_7 - u_8^2w_6w_8\right)\right]v_6v_5 - (t_5u_7v_5w_7 + t_6u_8v_6w_8)(t_1u_3v_2w_4 + t_2u_4v_1w_3),\end{aligned} \tag{B4}$$

$$\begin{aligned}E =& \left[u_8\left(t_6^2v_6v_8 - t_7^2v_5v_7\right)u_5 + u_6u_7\left(t_5^2v_5v_7 - t_8^2v_6v_8\right)\right]w_5w_6 - \left[t_7\left(-v_5^2w_6w_7 + v_7^2w_5w_8\right)t_5 - t_6t_8\left(v_6^2w_5w_8 - v_8^2w_6w_7\right)\right]u_5u_6\\ &\times \left[t_8\left(-u_6^2w_6w_8 + u_7^2w_5w_7\right)t_5 - t_6t_7\left(u_5^2w_5w_7 - u_8^2w_6w_8\right)\right]v_7v_8 - \left[-u_7\left(v_5v_8w_7^2 - v_6v_7w_5^2\right)u_5\right.\\ &\left.+ u_6u_8\left(v_5v_8w_6^2 - v_6v_7w_8^2\right)\right]t_8t_7 - (t_1u_3v_2w_4 + t_2u_4v_1w_3)(t_7u_5v_7w_5 + t_8u_6v_8w_6),\end{aligned} \tag{B5}$$

$$F = t_5t_6u_7u_8v_7v_8w_5w_6 + t_7t_8u_5u_6v_5v_6w_7w_8 + (v_5v_8w_6w_7 + v_6v_7w_5w_8)(t_5t_8u_6u_7 + t_6t_7u_5u_8), \tag{B6}$$

$$G = t_5t_6u_5u_6v_5v_6w_5w_6 + t_7t_8u_7u_8v_7v_8w_7w_8 + (u_5u_7w_5w_7 + u_6u_8w_6w_8)(t_5t_7v_5v_7 + t_6t_8v_6v_8), \tag{B7}$$

$$H = -w_7w_8v_5v_6(t_5t_8u_6u_7 + t_6t_7u_5u_8) - u_7u_8t_5t_6(v_5v_8w_6w_7 + v_6v_7w_5w_8), \tag{B8}$$

$$I = -w_5w_6v_7v_8(t_5t_8u_6u_7 + t_6t_7u_5u_8) - u_5u_6t_7t_8(v_5v_8w_6w_7 + v_6v_7w_5w_8), \tag{B9}$$

$$J = -u_7u_8w_7w_8(t_5t_7v_5v_7 + t_6t_8v_6v_8) - v_5v_6t_5t_6(u_5u_7w_5w_7 + u_6u_8w_6w_8), \tag{B10}$$

$$K = -u_5u_6w_5w_6(t_5t_7v_5v_7 + t_6t_8v_6v_8) - v_7v_8t_7t_8(u_5u_7w_5w_7 + u_6u_8w_6w_8), \tag{B11}$$

$$L = t_5t_6u_7u_8v_5v_6w_7w_8, \tag{B12}$$

$$M = t_7t_8u_5u_6v_7v_8w_5w_6. \tag{B13}$$

2. Trapezoid free energy

The trapezoid free energy can be specialized from the bipartite staggered odd eight-vertex model [53] rather than the four-unit staggered odd eight-vertex model, and it is of the form

$$\begin{aligned}-\beta f_{\mathrm{T}} =& \frac{1}{16\pi^2}\int_0^{2\pi}\int_0^{2\pi} \ln[A + 2B\cos(\theta_1) + 2C\cos(\theta_2) + 2D\cos(\theta_1+\theta_2) + 2G\cos(2\theta_2) + 2J\cos(\theta_1+2\theta_2)\\ &+ 2L\cos(2\theta_1+2\theta_2)]d\theta_1 d\theta_2,\end{aligned} \tag{B14}$$

where

$$A = v_3^2 w_1^2 + 2v_3 v_4 w_1 w_2 + v_4^2 w_2^2 + v_5^2 w_7^2 + v_6^2 w_8^2 + v_7^2 w_5^2 + v_8^2 w_6^2, \tag{B15}$$

$$B = -v_5 v_7 w_5 w_7 - v_6 v_8 w_6 w_8, \tag{B16}$$

$$C = (v_3 w_1 + v_4 w_2)(v_7 w_5 + v_8 w_6), \tag{B17}$$

$$D = -(v_3 w_1 + v_4 w_2)(v_5 w_7 + v_6 w_8), \tag{B18}$$

$$G = v_7 v_8 w_6 w_5, \tag{B19}$$

$$J = -v_5 v_8 w_6 w_7 - v_6 v_7 w_5 w_8, \tag{B20}$$

$$L = v_5 v_6 w_7 w_8. \tag{B21}$$

3. Barreto's Mars free energy

The Barreto's Mars free energy can be specialized from the full four-unit column staggered odd eight-vertex model. There is a vast simplification so that only the A term in the integrand is nonzero, giving the simple free-energy expression

$$-\beta f_{\mathrm{Ma}} = \tfrac{1}{8} \ln[(t_1 u_3 v_2 w_4 + t_2 u_4 v_1 w_3 + t_5 u_6 v_7 w_8 + t_6 u_5 v_8 w_7)^2 - 2u_3 u_4 w_3 w_4 (t_1 t_2 v_1 v_2 - t_5 t_6 v_7 v_8)]. \tag{B22}$$

Upon expanding the argument of the logarithm, we see that all of the terms are positive.

4. Kite free energy

The kite model free energy can be specialized from the trapezoid free energy, giving

$$-\beta f_{\mathrm{K}} = \frac{1}{16\pi^2} \int_0^{2\pi} \int_0^{2\pi} \ln[A + 2C\cos(\theta_2) + 2G\cos(2\theta_2)] d\theta_1 d\theta_2, \tag{B23}$$

where

$$A = v_1^2 w_3^2 + v_2^2 w_4^2 + v_7^2 w_5^2 + 2v_7 v_8 w_5 w_6 + v_8^2 w_6^2, \tag{B24}$$

$$C = (v_7 w_5 + v_8 w_6)(v_1 w_3 + v_2 w_4), \tag{B25}$$

$$G = w_3 w_4 v_7 v_8. \tag{B26}$$

We give in the main text an alternative derivation which does not require the free-fermion condition on each set of vertex weights.

5. Simple square free energies

The free energy of the general four-unit column staggered odd eight-vertex free-fermion model is quite large. As noted above, using mappings in [53], the expressions of [55] can alternatively be used to find the free energy of this most general case.

The four-unit free energy can be specialized to the column and bipartite staggered odd eight-vertex models with units of two vertices, but we instead use the derivation of [53]. The respective free energies are given as [53]

$$-\beta f_{\mathrm{SC}} = \frac{1}{16\pi^2} \int_0^{2\pi} \int_0^{2\pi} \ln[A + 2B\cos(\theta_1) + 2C\cos(\theta_2) + 2D\cos(\theta_1 - \theta_2) + 2E\cos(\theta_1 + \theta_2) + 2G\cos(2\theta_2) + 2H\cos(\theta_1 - 2\theta_2) + 2I\cos(\theta_1 + 2\theta_2)] d\theta_1 d\theta_2, \tag{B27}$$

$$A = \left(v_5^2 + v_8^2\right)\left(w_6^2 + w_7^2\right) + \left(v_6^2 + v_7^2\right)\left(w_5^2 + w_8^2\right) + 2v_1 v_3 w_1 w_3 + 2v_2 v_4 w_2 w_4 + 2v_5 v_8 w_6 w_7 + 2v_6 v_7 w_5 w_8, \tag{B28}$$

$$B = v_1 v_2 w_3 w_4 + v_3 v_4 w_1 w_2 - v_5 v_6 w_7 w_8 - v_7 v_8 w_5 w_6 - (v_5 v_7 - v_6 v_8)(w_5 w_7 - w_6 w_8), \tag{B29}$$

$$C = w_5 w_8 \left(v_6^2 + v_7^2\right) - w_6 w_7 \left(v_5^2 + v_8^2\right) - v_5 v_8 \left(w_6^2 + w_7^2\right) + v_6 v_7 \left(w_5^2 + w_8^2\right), \tag{B30}$$

$$D = (v_3 v_4 - v_5 v_6)(w_5 w_7 - w_6 w_8) - (v_5 v_7 - v_6 v_8)(w_3 w_4 - w_5 w_6), \tag{B31}$$

$$E = (v_1 v_2 - v_5 v_6)(w_5 w_7 - w_6 w_8) - (v_5 v_7 - v_6 v_8)(w_1 w_2 - w_5 w_6), \tag{B32}$$

$$G = v_8 v_5 w_7 w_6 + v_7 v_6 w_8 w_5 - v_3 v_1 w_3 w_1 - v_4 v_2 w_4 w_2, \tag{B33}$$

$$H = (v_1 v_2 - v_7 v_8)(w_1 w_2 - w_7 w_8), \tag{B34}$$

$$I = (v_1 v_2 - v_5 v_6)(w_1 w_2 - w_5 w_6) \tag{B35}$$

and

$$-\beta f_{\mathrm{SB}} = \frac{1}{16\pi^2} \int_0^{2\pi} \int_0^{2\pi} \ln[A + 2B\cos(\theta_1) + 2C\cos(\theta_2) + 2D\cos(\theta_1 - \theta_2) + 2E\cos(\theta_1 + \theta_2) + 2F\cos(2\theta_1) + 2G\cos(2\theta_2)] d\theta_1 d\theta_2, \tag{B36}$$

$$A = w_8^2 v_6^2 + w_7^2 v_5^2 + w_5^2 v_7^2 + w_6^2 v_8^2 + w_3^2 v_1^2 + w_4^2 v_2^2 + w_1^2 v_3^2 + w_2^2 v_4^2 + 2(v_8 v_7 + v_5 v_6)(w_8 w_7 + w_5 w_6), \tag{B37}$$

$$B = (v_1w_3 + v_2w_4)(v_7w_5 + v_8w_6) - (v_3w_1 + v_4w_2)(v_5w_7 + v_6w_8), \tag{B38}$$

$$C = (v_3w_1 + v_4w_2)(v_7w_5 + v_8w_6) - (v_1w_3 + v_2w_4)(v_5w_7 + v_6w_8), \tag{B39}$$

$$D = v_1v_4w_2w_3 + v_2v_3w_1w_4 - v_6v_8w_6w_8 - v_5v_7w_5w_7, \tag{B40}$$

$$E = v_1v_3w_1w_3 + v_2v_4w_2w_4 - v_6v_7w_5w_8 - v_5v_8w_6w_7, \tag{B41}$$

$$F = -(v_1v_2 - v_5v_6)(w_1w_2 - w_5w_6), \tag{B42}$$

$$G = -(v_1v_2 - v_7v_8)(w_1w_2 - w_7w_8). \tag{B43}$$

Both of these free energies can be specialized to the homogeneous lattice, giving [52,53]

$$-\beta f_S = \frac{1}{8\pi^2}\int_0^{2\pi}\int_0^{2\pi} d\theta_1 d\theta_2 \ln[A + 2B\cos(\theta_1) + 2C\cos(\theta_2) + 2D\cos(\theta_1 - \theta_2) + 2E\cos(\theta_1 + \theta_2)], \tag{B44}$$

$$A = (v_1v_2 + v_3v_4)(v_5v_6 + v_7v_8) + v_1^2v_4^2 + v_2^2v_3^2 + v_5^2v_7^2 + v_6^2v_8^2, \tag{B45}$$

$$B = 2v_5v_6v_7v_8 - v_1^2v_4^2 - v_2^2v_3^2, \tag{B46}$$

$$C = 2v_1v_2v_3v_4 - v_5^2v_7^2 - v_6^2v_8^2, \tag{B47}$$

$$D = (v_1v_2 - v_7v_8)(v_5v_6 - v_3v_4), \tag{B48}$$

$$E = (v_1v_2 - v_5v_6)(v_7v_8 - v_3v_4). \tag{B49}$$

[1] E. Hawkes, B. An, N. M. Benbernou, H. Tanaka, S. Kim, E. D. Demaine, D. Rus, and R. J. Wood, Programmable matter by folding, Proc. Natl. Acad. Sci. U.S.A. **107**, 12441 (2010).

[2] B. An, N. Benbernou, E. D. Demaine, and D. Rus, Planning to fold multiple objects from a single self-folding sheet, Robotica **29**, 87 (2011).

[3] J. L. Silverberg, A. A. Evans, L. McLeod, R. C. Hayward, T. Hull, C. D. Santangelo, and I. Cohen, Using origami design principles to fold reprogrammable mechanical metamaterials, Science **345**, 647 (2014).

[4] L. H. Dudte, E. Vouga, T. Tachi, and L. Mahadevan, Programming curvature using origami tessellations, Nat. Mater. **15**, 583 (2016).

[5] S. M. Felton, M. T. Tolley, B. Shin, C. D. Onal, E. D. Demaine, D. Rus, and R. J. Wood, Self-folding with shape memory composites, Soft. Matter **9**, 7688 (2013).

[6] M. T. Tolley, S. M. Felton, S. Miyashita, D. Aukes, D. Rus, and R. J. Wood, Self-folding origami: Shape memory composites activated by uniform heating, Smart Mater. Struct. **23**, 094006 (2014).

[7] T. Tachi, *Proceedings of the International Association for Shell and Spatial Structures (IASS) Symposium, Shanghai, 2010* (Elsevier, Amsterdam, 2010), Vol. 12, pp. 458–460.

[8] T. S. Shim, S.-H. Kim, C.-J. Heo, H. C. Jeon, and S.-M. Yang, Controlled origami folding of hydrogel bilayers with sustained reversibility for robust microcarriers, Angew. Chem. Int. Ed. **51**, 1420 (2012).

[9] C. L. Randall, E. Gultepe, and D. H. Gracias, Self-folding devices and materials for biomedical applications, Trends Biotechnol. **30**, 138 (2012).

[10] R. Fernandes and D. H. Gracias, Self-folding polymeric containers for encapsulation and delivery of drugs, Adv. Drug Delivery Rev. **64**, 1579 (2012).

[11] D. H. Gracias, Stimuli responsive self-folding using thin polymer films, Curr. Opin. Chem. Eng. **2**, 112 (2013).

[12] J. L. Silverberg, J.-H. Na, A. A. Evans, B. Liu, T. C. Hull, C. D. Santangelo, R. J. Lang, R. C. Hayward, and I. Cohen, Origami structures with a critical transition to bistability arising from hidden degrees of freedom, Nat. Mater. **14**, 389 (2015).

[13] J.-H. Na, A. A. Evans, J. Bae, M. C. Chiappelli, C. D. Santangelo, R. J. Lang, T. C. Hull, and R. C. Hayward, Programming reversibly self-folding origami with micropatterned photocrosslinkable polymer trilayers, Adv. Mater. **27**, 79 (2015).

[14] J. M. Z. Ocampo, P. O. Vaccaro, T. Fleischmann, T.-S. Wang, K. Kubota, T. Aida, T. Ohnishi, A. Sugimura, R. Izumoto, M. Hosoda, and S. Nashima, Optical actuation of micromirrors fabricated by the micro-origami technique, Appl. Phys. Lett. **83**, 3647 (2003).

[15] M. C. Mulakkal, A. M. Seddon, G. Whittell, I. Manners, and R. S. Trask, 4D fibrous materials: Characterising the deployment of paper architectures, Smart Mater. Struct. **25**, 095052 (2016).

[16] E. A. Peraza-Hernandez, D. J. Hartl, R. J. Malak, Jr., and D. C. Lagoudas, Origami-inspired active structures: A synthesis and review, Smart Mater. Struct. **23**, 094001 (2014).

[17] A. A. Evans (private communication).

[18] B. Ballinger, M. Damian, D. Eppstein, R. Flatland, J. Ginepro, and T. Hull, *Proceedings of the 26th Annual ACM-SIAM Symposium on Discrete Algorithms, SODA '15* (SIAM, Philadelphia, 2015), pp. 136–147.

[19] Z. Abel, J. Cantarella, E. D. Demaine, D. Eppstein, T. C. Hull, J. S. Ku, R. J. Lang, and T. Tachi, Rigid origami vertices: Conditions and forcing sets, J. Comput. Geom. **7**, 171 (2016).

[20] S. Waitukaitis, R. Menaut, B. G.-g. Chen, and M. van Hecke, Origami Multistability: From Single Vertices to Metasheets, Phys. Rev. Lett. **114**, 055503 (2015).

[21] M. Stern, M. Pinson, and A. Murugan, The Difficulty of Folding Self-Folding Origami, Phys. Rev. X **7**, 041070 (2017).

[22] E. Demaine and J. O'Rourke, *Geometric Folding Algorithms: Linkages, Origami, Polyhedra* (Cambridge University Press, Cambridge, 2007).

[23] T. A. Evans, R. J. Lang, S. P. Magleby, and L. L. Howell, Rigidly foldable origami gadgets and tessellations, R. Soc. Open Sci. **2**, 150067 (2015).

[24] M. Bern and B. Hayes, *Proceedings of the Seventh Annual ACM-SIAM Symposium on Discrete Algorithms, SODA '96* (SIAM, Philadelphia, 1996), pp. 175–183.

[25] S. Mori and Y. Kajinaga, Square lattice with attractive interactions, Phys. Rev. E **53**, 124 (1996).

[26] P. Di Francesco and E. Guitter, Folding transition of the triangular lattice, Phys. Rev. E **50**, 4418 (1994).

[27] M. Bowick, P. Di Francesco, O. Golinelli, and E. Guitter, Three-dimensional folding of the triangular lattice, Nucl. Phys. B **450**, 463 (1995).

[28] C. Münkel and D. W. Heermann, Folding Transitions of Self-Avoiding Membranes, Phys. Rev. Lett. **75**, 1666 (1995).

[29] M. Bowick, P. Di Francesco, O. Golinelli, and E. Guitter, *Proceedings of the Fourth Chia Meeting on Condensed Matter and High Energy Physics* (World Scientific, Singapore, 1996).

[30] E. N. M. Cirillo, G. Gonnella, and A. Pelizzola, Folding transitions of the triangular lattice with defects, Phys. Rev. E **53**, 1479 (1996).

[31] E. N. M. Cirillo, G. Gonnella, and A. Pelizzola, Folding transition of the triangular lattice in a discrete three-dimensional space, Phys. Rev. E **53**, 3253 (1996).

[32] S. Mori and S. Komura, Monte Carlo study of a self-avoiding polymerized membrane with negative bending rigidity, J. Phys. A: Math. Gen. **29**, 7439 (1996).

[33] P. Di Francesco, E. Guitter, and S. Mori, Folding of the triangular lattice with quenched random bending rigidity, Phys. Rev. E **55**, 237 (1997).

[34] M. Bowick, O. Golinelli, E. Guitter, and S. Mori, Geometrical folding transitions of the triangular lattice in the face-centred cubic lattice, Nucl. Phys. B **495**, 583 (1997).

[35] S. Mori and E. Guitter, Folding of the triangular lattice in the face-centred cubic lattice with quenched random spontaneous curvature, J. Phys. A: Math. Gen. **30**, L829 (1997).

[36] H. Popova and A. Milchev, Structure, dynamics, and phase transitions of tethered membranes: A Monte Carlo simulation study, J. Chem. Phys. **127**, 194903 (2007).

[37] H. Popova and A. Milchev, Structure, dynamic properties, and phase transitions of tethered membranes, Ann. N.Y. Acad. Sci. **1161**, 397 (2009).

[38] P. Di Francesco, Folding transitions of the square-diagonal lattice, Nucl. Phys. B **528**, 453 (1998).

[39] P. Di Francesco, Folding the square-diagonal lattice, Nucl. Phys. B **525**, 507 (1998).

[40] E. N. M. Cirillo, G. Gonnella, and A. Pelizzola, Folding transitions of the square-diagonal two-dimensional lattice, Nucl. Phys. B **583**, 584 (2000).

[41] P. Di Francesco, O. Golinelli, and E. Guitter, Meander, folding, and arch statistics, Math. Comput. Model. **26**, 97 (1997).

[42] P. Di Francesco, O. Golinelli, and E. Guitter, Meanders and the Temperley-Lieb algebra, Commun. Math. Phys. **186**, 1 (1997).

[43] P. Di Francesco, B. Eynard, and E. Guitter, Coloring random triangulations, Nucl. Phys. B **516**, 543 (1998).

[44] P. Di Francesco, in *Random Matrix Models and Their Applications*, edited by P. Bleher and A. Its (Cambridge University Press, Cambridge, 2001), Vol. 40, pp. 111–170.

[45] P. Di Francesco, Folding and coloring problems in mathematics and physics, Bull. Am. Math. Soc. **37**, 251 (2000).

[46] M. J. Bowick and A. Travesset, The statistical mechanics of membranes, Phys. Rep. **344**, 255 (2001).

[47] P. Di Francesco and E. Guitter, Geometrically constrained statistical systems on regular and random lattices: From folding to meanders, Phys. Rep. **415**, 1 (2005).

[48] E. F. Shender, V. B. Cherepanov, P. C. W. Holdsworth, and A. J. Berlinsky, Kagomé Antiferromagnet with Defects: Satisfaction, Frustration, and Spin Folding in a Random Spin System, Phys. Rev. Lett. **70**, 3812 (1993).

[49] P. Di Francesco and E. Guitter, Entropy of folding of the triangular lattice, Europhys. Lett. **26**, 455 (1994).

[50] J. Ginepro and T. C. Hull, Counting Miura-ori foldings, J. Integer Sequences **17**, 8 (2014).

[51] R. J. Lang (private communication).

[52] F. Y. Wu and H. Kunz, The odd eight-vertex model, J. Stat. Phys. **116**, 67 (2004).

[53] M. Assis, The 16-vertex model and its even and odd 8-vertex subcases on the square lattice, J. Phys. A: Math. Theor. **50**, 395001 (2017).

[54] C. S. Hsue, K. Y. Lin, and F. Y. Wu, Staggered eight-vertex model, Phys. Rev. B **12**, 429 (1975).

[55] K. Y. Lin and I. P. Wang, Staggered eight-vertex model with four sublattices, J. Phys. A: Math. Gen. **10**, 813 (1977).

[56] R. J. Baxter, Three-colorings of the square lattice: A hard squares model, J. Math. Phys. **11**, 3116 (1970).

[57] N. E. Pegg, The generalised six-vertex model, J. Phys. A: Math. Gen. **15**, L549 (1982).

[58] P. A. Pearce and K. A. Seaton, Exact solution of cyclic solid-on-solid lattice models, Ann. Phys. (N.Y.) **193**, 326 (1989).

[59] F. Y. Wu, Exact results on a general lattice statistical model, Solid State Commun. **10**, 115 (1972).

[60] B. McCoy and T. T. Wu, *The Two-Dimensional Ising Model* (Harvard University Press, Cambridge, 1973).

[61] B. McCoy and T. T. Wu, *The Two-Dimensional Ising Model*, 2nd ed. (Dover, New York, 2014).

[62] C. Fan and F. Y. Wu, General Lattice Model of Phase Transitions, Phys. Rev. B **2**, 723 (1970).

[63] R. Baxter, *Exactly Solved Models in Statistical Mechanics* (Academic, New York, 1982).

[64] R. Baxter, *Exactly Solved Models in Statistical Mechanics* (Dover, New York, 2007).

[65] D. S. Gaunt and M. E. Fisher, Hard-sphere lattice gases. I. Plane-square lattice, J. Chem. Phys. **43**, 2840 (1965).

[66] L. K. Runnels and L. L. Combs, Exact finite method of lattice statistics. I. Square and triangular lattice gases of hard molecules, J. Chem. Phys. **45**, 2482 (1966).

[67] Y.-b. Chan, Series expansions from the corner transfer matrix renormalization group method: The hard-squares model, J. Phys. A: Math. Theor. **45**, 085001 (2012).

[68] Y.-b. Chan, Series expansions from the corner transfer matrix renormalization group method: II. Asymmetry and high-density hard squares, J. Phys. A: Math. Theor. **46**, 125009 (2013).

[69] T. Deguchi, Multivariable vertex models associated with the Temperley-Lieb algebra, Phys. Lett. A **159**, 163 (1991).

[70] T. Tachi, *Generalization of Rigid Foldable Quadrilateral Mesh Origami* (Editorial Universitat Politècnica de València, València, 2009), pp. 2287–2294.

[71] T. Tachi, *One-DOF Cylindrical Deployable Structures with Rigid Quadrilateral Panels* (Editorial Universitat Politècnica de València, València, 2010), pp. 2295–2305.

[72] T. Tachi, Design of infinitesimally and finitely flexible origami based on reciprocal figures, J. Geom. Graphics **16**, 223 (2012).

[73] T. Tachi and T. C. Hull, Self-foldability of rigid origami, J. Mech. Robot. **9**, 021008 (2017).

[74] R. J. Lang, S. Magleby, and L. Howell, Single degree-of-freedom rigidly foldable cut origami flashers, J. Mech. Robot. **8**, 031005 (2016).

[75] B. M. McCoy and T. T. Wu, Theory of Toeplitz determinants and the spin correlations of the two-dimensional Ising model. II, Phys. Rev. **155**, 438 (1967).

[76] A. G. Izergin and V. E. Korepin, The inverse scattering method approach to the quantum Shabat-Mikhailov model, Commun. Math. Phys. **79**, 303 (1981).

[77] H. S. Green and C. A. Hurst, *Order-Disorder Phenomena*, Monographs in Statistical Physics and Thermodynamics Vol. 5 (Interscience, New York, 1964).

[78] C. A. Hurst, Solution of plane Ising lattices by the Pfaffian method, J. Chem. Phys. **38**, 2558 (1963).

[79] J. E. Sacco and F. Y. Wu, 32-vertex model on the triangular lattice, J. Phys. A: Math. Gen. **8**, 1780 (1975).

[80] J. E. Sacco and F. Y. Wu, 32-vertex model on the triangular lattice, J. Phys. A: Math. Gen. **10**, 1259 (1977).